Research Article **Open Access**

Jaydeep P. Bardhan*, Matthew G. Knepley, and Peter Brune

Nonlocal Electrostatics in Spherical Geometries Using Eigenfunction Expansions of Boundary-Integral Operators

Abstract: In this paper, we present an exact, infinite-series solution to Lorentz nonlocal continuum electrostatics for an arbitrary charge distribution in a spherical solute. Our approach relies on two key steps: (1) re-formulating the PDE problem using boundary-integral equations, and (2) diagonalizing the boundary-integral operators using the fact that their eigenfunctions are the surface spherical harmonics. To introduce this uncommon approach for calculations in separable geometries, we first re-derive Kirkwood's classic results for a protein surrounded concentrically by a pure-water ion-exclusion (Stern) layer and then a dilute electrolyte, which is modeled with the linearized Poisson–Boltzmann equation. The eigenfunction-expansion approach provides a computationally efficient way to test some implications of nonlocal models, including estimating the reasonable range of the nonlocal length-scale parameter λ. Our results suggest that nonlocal solvent response may help to reduce the need for very high dielectric constants in calculating pH-dependent protein behavior, though more sophisticated nonlocal models are needed to resolve this question in full. An open-source MATLAB implementation of our approach is freely available online.

DOI 10.1515/mlbmb-2015-0001
Received August 24, 2014; accepted December 11, 2014

1 Introduction

One of the long-standing challenges in molecular biophysics is the development of accurate, yet simple models for the influence of biological fluids (aqueous solutions composed of water and dissolved ions) on biological molecules such as proteins and DNA. Atomistic simulations that include explicit water molecules, for instance molecular dynamics (MD), provide the most detailed molecular understanding that is widely accessible without specialized computational resources. However, these simulations come at two prices: first, MD simulations can require many hundreds of compute hours, most of which are spent on the thousands of water molecules whose individual behaviors are not of primary relevance; second, practitioners must understand numerous subtleties about simulation protocols and the parameters associated with the physical models (force fields). Implicit-solvent models replace the explicit water molecules with an approximation to the theoretically rigorous potential of mean force (PMF) [1], creating the possibility of simulating molecular behavior accurately but orders of magnitude faster, and with fewer statistical uncertainties. Unfortunately, the statistical mechanical derivation of the PMF is not constructive, in the sense that the derivation does not provide a general PMF suitable for all molecular solutes. Instead, one must guess a functional form for the electrostatic interactions between solvent and solute, find the optimal parameters, and then test its fit against real data (both experiment and more accurate theories such as MD).

***Corresponding Author: Jaydeep P. Bardhan:** Dept. of Mechanical and Industrial Engineering, Northeastern University, Boston MA 02115
Matthew G. Knepley: Computation Institute, University of Chicago, Chicago IL 60637
Peter Brune: Google Inc., Mountain View CA 94041

Of course, evaluation of an implicit-solvent model is greatly accelerated if it can be solved easily and rapidly on relevant, non-trivial problems. With the advent of fast computers, one reasonable option is to make numerical software implementing the new model freely available online [2, 3]. Another option is to provide analytical solutions for tractable geometries. Spheres are frequently used for continuum electrostatic modeling, because exact results can be obtained using spherical harmonics and the method of separation of variables [4, 5]. Kirkwood's classic solution for a spherical protein embedded in a dilute electrolyte represents the best-known example [4], and demonstrates this conceptually simple approach. One merely writes down spherical-harmonic expansions and matches expansion coefficients using the known boundary conditions. Even though proteins obviously have complicated shapes, analysis of spherical geometries can offer insights into problems such as pK_a predictions [6], redox potentials [7], strategies for optimizing molecular binding [8], and fast analytical models such as Generalized Born [9, 66].

However, Kirkwood's work also demonstrates a difficulty with the approach: as one adds detail to the model—in Kirkwood's case, an ion-exclusion layer outside the protein—calculations become onerously complex very quickly. In addition, modeling the linearized Poisson–Boltzmann equation in the solvent necessitated the introduction of a set of polynomials for the radial coordinate because the standard Bessel functions were unsuitable [4]; more than sixty years passed before the relationship between Kirkwood's polynomials and the Bessel functions was established, allowing at the end a substantial simplification [10].

In this paper, we present an alternative strategy for obtaining analytical solutions in separable geometries. The first step is to transform the given system of partial-differential equations (PDEs) into one of boundary-integral equations (BIEs) [11], so that the unknowns are no longer functions defined over three-dimensional regions of space, but instead functions defined on two-dimensional boundaries. This reformulation removes the complications associated with using Bessel functions in the solvent electrolyte volume. Second, the boundary-integral operators are diagonalized using the appropriate harmonics [12, 13]. This allows a mode-by-mode calculation of the unknown functions on the boundary in terms of the appropriate *surface* harmonics—in contrast to matched-expansion approaches that employ *solid* harmonics. To demonstrate the BIE-eigenfunction approach, we solve the Kirkwood problem (a spherical protein embedded in a dilute electrolyte, with a thin ion-exclusion or Stern layer [4]) and derive the full solution to the more recent nonlocal-dielectric model of Dogonadze and Kornyshev [14, 15].

The nonlocal model was originally developed to address one of the key shortcomings of macroscopic continuum theories for molecular solvation: the fact that the solvent molecules (usually water) are not infinitesimally small compared to length scales of interest, e.g., small ions [16, 17] and proteins [18]. Unfortunately, nonlocal response means that even the simplest form of the nonlocal model, called the Lorentz nonlocal theory [19], leads to an integrodifferential Poisson equation, which is difficult to solve analytically or even numerically. The only readily solved geometries for the Lorentz nonlocal model have been the sphere with central charge [20, 21] and the charge near a half-space [18, 22, 23], and no numerical algorithms for the original nonlocal model in arbitrary geometries were ever presented. Although Vorotyntsev and Kornyshev presented a possible general formalism [15], which enabled a solution for arbitrary charges in a sphere [24], the analytical approach has not been widely adopted.

Very recently, however, Hildebrandt and collaborators derived several mathematical reformulations to render the Lorentz nonlocal electrostatic model tractable both analytically and computationally [17, 25–27]. The first major step was reformulating the nonlocal integrodifferential Poisson problem in one unknown variable, the electrostatic potential $\varphi(\mathbf{r})$, as a pair of coupled, purely local PDEs with two unknown variables throughout space ($\varphi(\mathbf{r})$ and an additional auxiliary potential) [17]. Similar reformulations of nonlocal continuum theory were obtained independently in other areas of physics [28–30]. Following reformulation, Green's theorem and double reciprocity can be used to transform the coupled PDE system into a purely boundary-integral-equation (BIE) representation of the nonlocal model [26, 31].

In principle, both the local-formulation PDE problem and the purely BIE method are solved problems numerically, in the sense that asymptotically optimal (linear-scaling) numerical algorithms exist [27, 32–36]. However, even "fast solvers" can require an hour or more of computation, and therefore analytical solutions of non-trivial problems still hold significant value in this relatively early stage of testing nonlocal electrostatics of molecular solvation. One application of analytical methods is to obtain qualitative insight into the

differences between nonlocal and local models using visualization: analytical methods allow rapid calculations of the reaction potential induced throughout a model geometry by a chemical group in the protein, e.g. an amino acid side chain. Another application of analytical methods is to obtain quantitative information that may help to determine model parameters. For example, the nonlocal model includes an additional parameter beyond those of the standard local model. This parameter, denoted by λ, is an effective length scale that captures water's transition from behaving like a low-dielectric material at short length scales to more familiar high-dielectric, bulk-like behavior at longer length scales. Parameterization requires extensive simulation and testing, and fast calculations aid significantly.

To support the development and testing of nonlocal electrostatic models for biomolecule solvation, we present here the nonlocal-model analogue of Kirkwood's result: namely, an analytical approach for the electrostatic solvation free energy of an arbitrary charge distribution in a spherical solute embedded in a solvent modeled as a Lorentz nonlocal dielectric. Kirkwood's classic work continues to have impact decades after the advent of numerical simulations of the continuum electrostatic model [6, 9, 37], and the present work significantly enlarges the scope of nonlocal problems that can be studied analytically. We note that mobile ions such as sodium and potassium play crucial physiological roles and that the present work addresses only pure water solvent. However, the nonlocal theory can be extended easily to linearized Poisson–Boltzmann treatment of physiological electrolyte solutions [17, 38], and these extensions are the subject of ongoing work.

The remainder of the paper is organized as follows: the next section describes the local and nonlocal models, their reformulation as systems of boundary-integral equations, and the eigendecompositions of the associated boundary-integral operators. In Section 3 we introduce our BIE-eigenfunction strategy by rederiving the solution to Kirkwood's problem, and then apply the strategy to solve the nonlocal problem. In Section 4, we present several applications of the analytical solution, which illuminate important differences between local and nonlocal electrostatics, including the choice of solute dielectric constant and the sensitivity of the nonlocal results to the solvent length-scale parameter λ. The paper concludes in Section 5 with a brief summary and discussion.

2 Background

2.1 Kirkwood's Local-Response Electrostatic Model

Figure 1(a) is an illustration of the local-response model under consideration. We assume that the solute region I is a sphere of radius b, which is centered at the origin, and that the solute is at infinite dilution in a dilute aqueous electrolyte solvent. The solute charge distribution $\rho(\mathbf{r})$ is modeled as a set of Q discrete point charges contained within the sphere, the ith of which has value q_i and is situated at (r_i, θ_i, ϕ_i). The solute is treated as a homogeneous local-response dielectric with relative permittivity $\epsilon_{\text{protein}}$, i.e. inside the protein, the constitutive relation between the displacement and electric field is

$$\mathbf{D}_{\text{I}}(\mathbf{r}) = \epsilon_{\text{protein}}\epsilon_0\mathbf{E}_{\text{I}}(\mathbf{r}) \tag{1}$$

where as usual $\mathbf{E}(\mathbf{r}) = -\nabla\varphi(\mathbf{r})$ with φ the electrostatic potential. Substituting this constitutive relation into Gauss's law for dielectrics

$$\nabla \cdot \mathbf{D}_{\text{I}}(\mathbf{r}) = \rho(\mathbf{r}), \tag{2}$$

we see the electrostatic potential in region I satisfies the familiar Poisson equation

$$\nabla^2\varphi_{\text{I}}(\mathbf{r}) = -\frac{\rho(\mathbf{r})}{\epsilon_0\epsilon_{\text{protein}}}. \tag{3}$$

In a thin solvent layer surrounding the protein, we have water but no mobile ions; assuming that they are point charges in hard spheres of radius d, the ion density must be zero for $||\mathbf{r}|| < b + d$. Consequently, in this region (labeled II in Figure 1(a)) the potential satisfies a Laplace equation and we assume the permittivity is just that of pure water $\epsilon_{\text{water}} \approx 80$. Standard boundary conditions hold at the protein–solvent interface

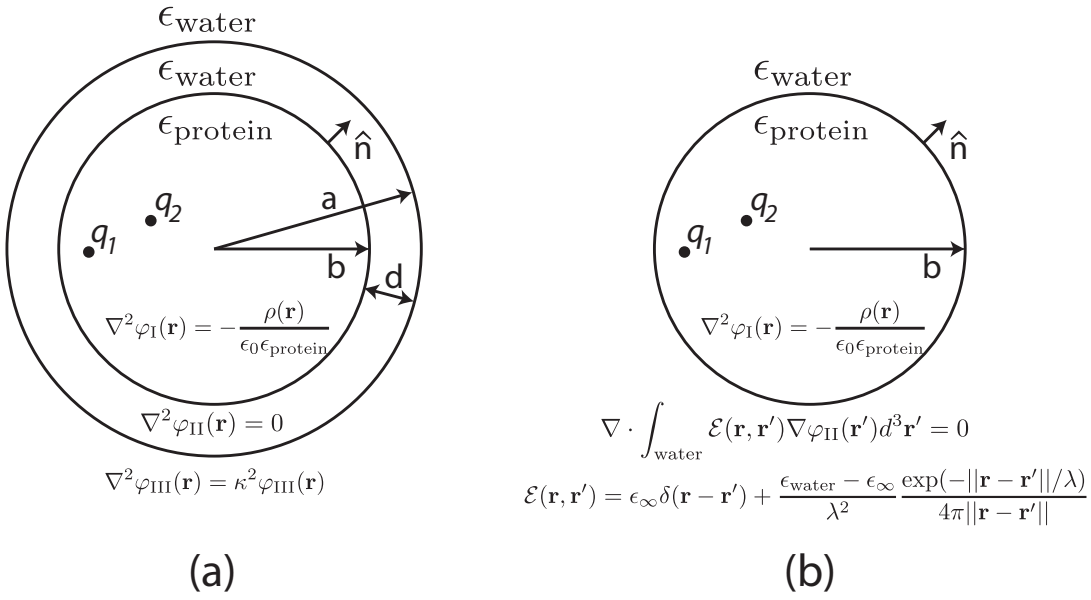

Figure 1: Diagram of the two continuum electrostatic models to be solved analytically. (a) Kirkwood's problem [4]. (b) Nonlocal-response model in a pure-water solvent.

defined by $||\mathbf{r}|| = b$, namely the continuity of the potential and the normal component of the displacement field:

$$\varphi_{\text{I}}(\mathbf{r}_b^-) = \varphi_{\text{II}}(\mathbf{r}_b^+) \tag{4}$$

$$\hat{\mathbf{n}} \cdot \mathbf{D}_{\text{I}}(\mathbf{r}_b^-) = \hat{\mathbf{n}} \cdot \mathbf{D}_{\text{II}}(\mathbf{r}_b^+). \tag{5}$$

For local-response dielectrics, Eq. 5 reduces to the familiar

$$\epsilon_{\text{protein}} \frac{\partial\varphi_{\text{I}}(\mathbf{r}_b^-)}{\partial n} = \epsilon_{\text{water}} \frac{\partial\varphi_{\text{II}}(\mathbf{r}_b^+)}{\partial n}. \tag{6}$$

where the normal direction $\hat{\mathbf{n}}$ points outward from region I to region II, we use the notation $\frac{\partial}{\partial n} = \hat{\mathbf{n}} \cdot \nabla$, and superscripts – and + denote interior (solute) and exterior (solvent) regions, respectively.

Outside this ion-exclusion layer, the mobile ions are assumed to redistribute such that at any point $\mathbf{r}$, the net charge density is the sum of the Boltzmann-weighted ion densities (i.e., neglecting the ion sizes and correlations between them). This leads to the nonlinear Poisson–Boltzmann equation, which here we simplify by linearization, i.e. the potential in region III satisfies the linearized Poisson–Boltzmann equation (LPBE)

$$\nabla^2\varphi_{\text{III}}(\mathbf{r}) = \kappa^2\varphi_{\text{III}}(\mathbf{r}) \tag{7}$$

where κ is the inverse Debye screening length; for physiological solutions, $\kappa^{-1} \approx 8$ Å. The electrolyte is also assumed to have relative permittivity ϵ_{water}, and so the boundary conditions at the ion-exclusion boundary Ω_a, defined as $||\mathbf{r}|| = a$, are

$$\varphi_{\text{II}}(\mathbf{r}_a^-) = \varphi_{\text{III}}(\mathbf{r}_a^+) \tag{8}$$

$$\frac{\partial\varphi_{\text{II}}(\mathbf{r}_a^-)}{\partial n} = \frac{\partial\varphi_{\text{III}}(\mathbf{r}_a^+)}{\partial n} \tag{9}$$

Kirkwood solved the above problem for the potential using matched expansions in the solid spherical harmonics [4]. Here, we show that an alternative is to use the surface harmonics for the BIE formulation of this problem, which may be derived as follows. For a point $\mathbf{r}$ in one of these regions, Green's representation theorem allows the potential at $\mathbf{r}$ to be written in terms of the potential and its normal derivative at the surface

or surfaces that bound the region [5, 35, 39, 40]. In region I, for example,

$$\varphi_{\mathrm{I}}(\mathbf{r}) = -\int_{\Omega_b} \frac{\partial G^L(\mathbf{r},\mathbf{r}')}{\partial n'}\varphi_{\mathrm{I}}(\mathbf{r}')dA' + \int_{\Omega_b} G^L(\mathbf{r},\mathbf{r}')\frac{\partial \varphi_{\mathrm{I}}(\mathbf{r}')}{\partial n'}dA' + \frac{1}{\epsilon_{\mathrm{protein}}}\int_{\text{region I}} G^L(\mathbf{r},\mathbf{r}')\rho(\mathbf{r}')dV', \tag{10}$$

where the subscript Ω_b denotes the spherical boundary $||\mathbf{r}|| = b$, $G^L(\mathbf{r},\mathbf{r}') = \frac{1}{4\pi||\mathbf{r}-\mathbf{r}'||}$ is the free-space Green's function for the Laplace equation, and the third term on the right-hand side represents the Coulomb potential induced by the solute charge distribution. Writing similar expressions for the potential in regions II and III, and taking careful limits as the field points approach these bounding surfaces, we obtain a system of four boundary-integral equations for the four unknown functions (the potential and normal derivative on the two boundaries). The complete derivation is presented elsewhere [35], but the final system may be written as

$$\begin{bmatrix} \frac{1}{2}I + K^L_{b,b} & -V^L_{b,b} & 0 & 0 \\ \frac{1}{2}I - K^L_{b,b} & \epsilon_{p,w}V^L_{b,b} & K^L_{b,a} & -V^L_{b,a} \\ -K^L_{a,b} & \epsilon_{p,w}V^L_{a,b} & \frac{1}{2}I + K^L_{a,a} & -V^L_{a,a} \\ 0 & 0 & \frac{1}{2}I - K^Y_{a,a} & V^Y_{a,a} \end{bmatrix} \begin{bmatrix} \phi_b \\ \frac{\partial\phi_b}{\partial n} \\ \phi_a \\ \frac{\partial\phi_a}{\partial n} \end{bmatrix} = \begin{bmatrix} \sum_{i=1}^{Q}\frac{q_i}{\epsilon_{\mathrm{protein}}}G^L \\ 0 \\ 0 \\ 0 \end{bmatrix}. \tag{11}$$

where I is the identity operator, and for domains Ω_x and Ω_y labeled x and y,

$$V^L_{x,y}\frac{\partial\varphi_y}{\partial n} = \int_{\Omega_y} G^L(\mathbf{r},\mathbf{r}')\frac{\partial\varphi(\mathbf{r}')}{\partial n'}dA', \qquad \mathbf{r}\in\Omega_x$$

$$K^L_{x,y}\varphi_y = \fint_{\Omega_y} \frac{\partial G^L(\mathbf{r},\mathbf{r}')}{\partial n'}\varphi(\mathbf{r}')dA', \qquad \mathbf{r}\in\Omega_x$$

and $\epsilon_{p,w} = \frac{\epsilon_{\mathrm{protein}}}{\epsilon_{\mathrm{water}}}$. Operators denoted with V are called single-layer potential operators (i.e., the second term on the right-hand side of Eq. 10) and those denoted K are referred to as double-layer potential operators (the first term on the right-hand side of Eq. 10). Note that the dash in the double-layer potential integral indicates that the integral should be understood in a Cauchy-principal value sense if the surfaces are the same (i.e. if $x = y$). The superscripts on these operators, L or Y, denote the Laplace or linearized Poisson–Boltzmann (Yukawa) Green's function, and the subscript pair x, y denotes the "source" surface (y) and the "destination" surface (x).

2.2 Nonlocal-Response Electrostatic Model

Figure 1(b) is an illustration of the nonlocal-response model. As in the local-response problem, we assume a spherical solute of radius b, centered at the origin, with Q discrete point charges as the solute charge distribution $\rho(\mathbf{r})$. We denote the one spherical boundary in the problem, which separates the protein and solvent, by b, and remind the reader that in this problem we are only treating a single boundary. Inside the protein, the total electrostatic potential $\varphi_{\mathrm{I}}(\mathbf{r})$ again obeys the familiar local-response dielectric theory with dielectric constant $\epsilon_{\mathrm{protein}}$:

$$\mathbf{E}_{\mathrm{I}}(\mathbf{r}) = -\nabla\varphi_{\mathrm{I}}(\mathbf{r}), \tag{12}$$

$$\mathbf{D}_{\mathrm{I}}(\mathbf{r}) = \epsilon_{\mathrm{protein}}\epsilon_0\mathbf{E}_{\mathrm{I}}(\mathbf{r}) \tag{13}$$

$$\nabla\cdot\mathbf{D}_{\mathrm{I}}(\mathbf{r}) = \rho(r). \tag{14}$$

We denote the Coulomb potential due to the fixed protein charges as

$$\varphi_{\mathrm{mol}} = \sum_{k=1}^{Q}\frac{q_k}{\epsilon_{\mathrm{protein}}|\mathbf{r}-\mathbf{r}_k|} \tag{15}$$

and the reaction potential due to the difference between the protein and solvent dielectric properties by φ_{reac}, the total electrostatic potential is

$$\varphi_{\mathrm{I}}(\mathbf{r}) = \varphi_{\mathrm{mol}}(\mathbf{r}) + \varphi_{\mathrm{reac}}(\mathbf{r}). \tag{16}$$

In this nonlocal problem, we have a pure water solvent (no mobile ions) in which the displacement and electric fields are related *nonlocally* by a convolution with a dielectric function of the form $\mathcal{E}(\mathbf{r},\mathbf{r}') = \epsilon(|\mathbf{r}-\mathbf{r}'|)$ so that

$$\mathbf{D}_{\mathrm{II}}(\mathbf{r}) = \epsilon_0 \int_{\text{region II}} \mathcal{E}(\mathbf{r},\mathbf{r}')\mathbf{E}_{\mathrm{II}}(\mathbf{r}')d^3\mathbf{r}' \tag{17}$$

$$\nabla\cdot\mathbf{D}_{\mathrm{II}}(\mathbf{r}) = 0, \tag{18}$$

and $\epsilon(|\mathbf{r}-\mathbf{r}'|)$ is the Lorentz nonlocal function

$$\mathcal{E}(\mathbf{r},\mathbf{r}') = \epsilon_\infty\delta(\mathbf{r}-\mathbf{r}') + \frac{\epsilon_{\text{water}}-\epsilon_\infty}{\lambda^2}\frac{\exp(-|\mathbf{r}-\mathbf{r}'|/\lambda)}{4\pi|\mathbf{r}-\mathbf{r}'|}, \tag{19}$$

where ϵ_{water} is the bulk solvent dielectric constant (80 in the present work), ϵ_∞ is the short-range dielectric constant, here taken to be the optical dielectric constant 1.8, and λ is an effective parameter that reflects the length scale associated with correlations between solvent molecules. At the solute–solvent interface b, the usual Maxwell boundary conditions Eqs. 4 and 5 apply. By Eqs. 17 and 18, the potential in the solvent must obey not the familiar Laplace equation but instead the integrodifferential equation

$$\nabla\cdot\int_{\text{region II}} \mathcal{E}(\mathbf{r},\mathbf{r}')\nabla\varphi_{\mathrm{II}}(\mathbf{r}')d^3\mathbf{r}' = 0, \tag{20}$$

the solution of which requires substantial calculation even for simple cases such as a sphere with central charge [16, 17, 20, 21, 25] or a charge approaching a planar half-space [17, 18, 22, 23].

Hildebrandt *et al.* recently reformulated this nonlocal model as a system of coupled but purely local partial differential equations (PDEs) [17]. Similar simplification strategies have been demonstrated for modeling dispersive electromagnetic media [28] and plasticity [29]. Essentially, for a nonlocal relationship that takes the form of a Green's function for a known PDE, one may be able to introduce a new unknown potential whose gradient is the vector field resulting from the convolution (here $\mathbf{D}_{\mathrm{II}}$). Enforcing the original conservation law (here, $\nabla\cdot\mathbf{D} = 0$) leads to an additional Laplace equation and then the original unknown interest and the additional unknown are coupled. For the Lorentzian model, the nonlocality resides in the second term of Eq. 19, which is merely the Green's function of the Yukawa equation $\nabla^2 u(\mathbf{r}) = \lambda^2 u(\mathbf{r})$. Here, by introducing the auxiliary displacement potential ψ_{II}, one may write the coupled PDE system as

$$\nabla^2\varphi_{\mathrm{I}}(\mathbf{r}) = -\rho(\mathbf{r}), \qquad \mathbf{r}\in\text{region I} \tag{21}$$

$$\nabla^2\psi_{\mathrm{II}}(\mathbf{r}) = 0, \qquad \mathbf{r}\in\text{region II} \tag{22}$$

$$\left(\nabla^2 - \frac{1}{\Lambda^2}\right)\varphi_{\mathrm{II}}(\mathbf{r}) = -\frac{1}{\lambda^2}\psi_{\mathrm{II}}(\mathbf{r}), \qquad \mathbf{r}\in\text{region II} \tag{23}$$

with $\Lambda = \lambda\sqrt{\epsilon_\infty/\epsilon_{\text{water}}}$. The exact displacement boundary condition (Eq. 5) is nonlocal and slow to compute, and so Hildebrandt [17] proposed the approximate boundary conditions

$$\varphi_{\mathrm{I}}(\mathbf{r}_b^-) = \varphi_{\mathrm{II}}(\mathbf{r}_b^+), \qquad \mathbf{r}_b\in\Omega_b \tag{24}$$

$$\epsilon_0\epsilon_{\text{protein}}\frac{\partial}{\partial n}\varphi_{\mathrm{I}}(\mathbf{r}_b^-) = \frac{\partial}{\partial n}\psi_{\mathrm{II}}(\mathbf{r}_b^+), \qquad \mathbf{r}_b\in\Omega_b \tag{25}$$

$$\frac{\partial}{\partial n}\psi_{\mathrm{II}}(\mathbf{r}_b^+) = \epsilon_0\epsilon_\infty\frac{\partial}{\partial n}\varphi_{\mathrm{II}}(\mathbf{r}_b^+), \qquad \mathbf{r}_b\in\Omega_b. \tag{26}$$

Different choices for boundary conditions are analyzed in more detail elsewhere, with model calculations suggesting that the impact on many calculations should be small compared to the overall differences between local and nonlocal models [21].

For numerical scaling, it is useful to change variables by introducing the substitution

$$\Psi = \frac{1}{\epsilon_\infty}\left(\frac{1}{\epsilon_0}\psi_{\mathrm{II}} - \epsilon_{\text{protein}}\varphi_{\text{mol}}\right), \tag{27}$$

as discussed extensively elsewhere [25]. Then, defining

$$\xi = -\left(\frac{1}{2}I - K_\Lambda^Y + \frac{\epsilon_{\text{protein}}}{\epsilon_{\text{water}}}K_\Lambda^{DR}\right)\varphi_{\text{mol}} - \left(\frac{\epsilon_{\text{protein}}}{\epsilon_\infty}V_\Lambda^Y - \frac{\epsilon_{\text{protein}}}{\epsilon_{\text{water}}}V_\Lambda^{DR}\right)\frac{\partial\varphi_{\text{mol}}}{\partial n}, \tag{28}$$

the complete BIE system is

$$\begin{bmatrix} \frac{1}{2}I - K_\Lambda^Y & -\frac{\epsilon_{\text{protein}}}{\epsilon_\infty}V_\Lambda^Y - \frac{\epsilon_{\text{protein}}}{\epsilon_{\text{water}}}V_\Lambda^{DR} & \frac{\epsilon_\infty}{\epsilon_{\text{water}}}K_\Lambda^{DR} \\ \frac{1}{2}I + K^L & -V^L & 0 \\ 0 & \frac{\epsilon_{\text{protein}}}{\epsilon_\infty}V^L & \frac{1}{2}I - K^L \end{bmatrix} \begin{bmatrix} \varphi_{\text{II}} \\ \frac{\partial\varphi_{\text{II}}}{\partial n} \\ \Psi \end{bmatrix} = \begin{bmatrix} \xi \\ 0 \\ 0 \end{bmatrix}, \tag{29}$$

where $V_\Lambda^{DR} = V_\Lambda^Y - V^L$, and similarly $K_\Lambda^{DR} = K_\Lambda^Y - K^L$. We omit the lengthy derivation and refer interested readers to Hildebrandt [25].

A point of great importance for fast numerical solution of Eq. 29 is that each non-zero block is a linear combination of the same boundary integral operators as are needed to solve Eq. 11. As a result, the same fast BEM solvers used for local electrostatics in the LPBE model (e.g., fast multipole methods [34], pre-corrected FFT [41], and the FFTSVD algorithm [35, 42]) can be adapted easily to solve nonlocal electrostatics models [36]. Fast solvers allow the discretized linear system, which is dense in the sense that the number of non-zero entries grows quadratically with the number of unknowns, to be solved in linear or near-linear time.

2.3 Eigenfunction Expansions of Boundary-Integral Operators on Spheres

All of the boundary-integral operators of Eqs. 11 and 29 are diagonalized by the surface spherical harmonics [43]. Consequently, the boundary integrals of the form $\int F(\mathbf{r}, \mathbf{r}')u(\mathbf{r}')dA'$ can be re-written as

$$\int_{\Omega_{\text{src}}} F(\mathbf{r}, \mathbf{r}')u(\mathbf{r}')dA' = \sum_{n=0}^{\infty}\sum_{m=-n}^{+n} Y_m^n(\theta, \phi)\lambda_{nm}^F \int_{\Omega_{\text{src}}} Y_m^{n,\star}(\theta', \phi')u(\theta', \phi')dA' \tag{30}$$

where the domain of integration Ω_{src} is the "source" surface (i.e. where the distribution of interest is located), (θ, ϕ) are the angular coordinates for $\mathbf{r}$, $Y_m^n(\theta, \phi)$ are the orthonormal surface harmonics, and λ_{nm}^F is the eigenvalue for the n, m mode of the operator F. Note that Eq. 30 represents a slight abuse of notation, in that the radii of the "source" and "destination" spheres are included only implicitly in the eigenvalues. Also, due to spherical symmetry, the eigenvalues of the relevant operators are independent of m, so we omit the second subscript in the remainder of the text.

For a sphere of radius R, the eigenvalues of the four "self-to-self" operators V^L, K^L, V^Y, and K^Y are

$$\lambda_n^{V^L} = \frac{R}{2n+1} \tag{31}$$

$$\lambda_n^{K^L} = -\frac{1}{2(2n+1)} \tag{32}$$

$$\lambda_n^{V^Y} = i(i\kappa)R^2 j_n(i\kappa R)h_n^{(1)}(i\kappa R) \tag{33}$$

$$\lambda_n^{K^Y} = i(i\kappa)^2 R^2/2\left(j_n(i\kappa R)h_n^{(1)}(i\kappa R)\right)' \tag{34}$$

where $i = \sqrt{-1}$, $j_n(x)$ and $h_n^{(1)}(x)$ denote the spherical Bessel function and spherical Hankel function of the first kind, respectively, and the prime notation in Eq. 34 denotes differentiation with respect to the argument.

The Kirkwood problem also involves four Laplace boundary-integral operators that map between concentric spheres. We demonstrate in Appendix A that the eigenvalues of these operators are

$$\lambda_n^{V^L_{a,b}} = \left(\frac{b}{a}\right)^{n+1} \frac{b}{2n+1} \tag{35}$$

$$\lambda_n^{K^L_{a,b}} = \begin{cases} 0, & n = 0 \\ -2n\left(\frac{b}{a}\right)^{n+1} \frac{-1}{2(2n+1)}, & n > 0 \end{cases} \tag{36}$$

$$\lambda_n^{V^L_{b,a}} = \left(\frac{a}{b}\right)^{n} \frac{a}{2n+1} \tag{37}$$

$$\lambda_n^{K^L_{b,a}} = \begin{cases} 1, & n = 0 \\ 2(n+1)\left(\frac{a}{b}\right)^{n} \frac{-1}{2(2n+1)}, & n > 0. \end{cases} \tag{38}$$

3 Eigenfunction Expansions of Boundary-Integral-Equation Formulations

3.1 Application to the Kirkwood Problem

To simplify the coupled boundary-integral equations, we introduce the spherical-harmonic projection operator $Y^\star$, which maps a function $u(\mathbf{r})$ defined on a sphere (i.e. in angular coordinates) into the expansion coefficients $\tilde{u} = [u_{n,m}]$ in the basis of surface spherical harmonics, which is complete and orthonormal:

$$Y^\star u(\mathbf{r}) = [u_{0,0}, u_{1,-1}, u_{1,0}, u_{1,1}, \ldots]^T \tag{39}$$

$$u_{n,m} = \int_{\Omega_{\text{src}}} Y_m^{n,\star}(\theta,\phi) u(\theta,\phi) dA. \tag{40}$$

Here again, the domain of integration Ω_{src} is the sphere on which u is defined. The operator Y, similarly, maps a vector of expansion coefficients in the basis of surface harmonics to a function on a given "destination" sphere, i.e. where the potential or its normal derivative is being evaluated:

$$u(\mathbf{r}) = Y\tilde{u} \tag{41}$$

$$u(\theta,\phi) = \sum_{n=0}^{\infty} \sum_{m=-n}^{+n} Y_m^n(\theta,\phi) u_{n,m}. \tag{42}$$

Using these definitions, the non-zero blocks of the matrix in Eq. 11 can be simultaneously diagonalized as

$$\begin{bmatrix} \frac{1}{2}I + D^{(1)} & -D^{(2)} & 0 & 0 \\ \frac{1}{2}I - D^{(1)} & \epsilon_{p,w} D^{(2)} & D^{(3)} & -D^{(4)} \\ -D^{(5)} & \epsilon_{p,w} D^{(6)} & \frac{1}{2}I + D^{(7)} & -D^{(8)} \\ 0 & 0 & \frac{1}{2}I - D^{(9)} & D^{(10)} \end{bmatrix}$$

$$= \begin{bmatrix} Y^\star & 0 & 0 & 0 \\ 0 & Y^\star & 0 & 0 \\ 0 & 0 & Y^\star & 0 \\ 0 & 0 & 0 & Y^\star \end{bmatrix} \begin{bmatrix} \frac{1}{2}I + K^L_{b,b} & -V^L_{b,b} & 0 & 0 \\ \frac{1}{2}I - K^L_{b,b} & \epsilon_{I,II} V^L_{b,b} & K^L_{b,a} & -V^L_{b,a} \\ -K^L_{a,b} & \epsilon_{I,II} V^L_{a,b} & \frac{1}{2}I + K^L_{a,a} & -V^L_{a,a} \\ 0 & 0 & \frac{1}{2}I - K^Y_{a,a} & V^Y_{a,a} \end{bmatrix} \begin{bmatrix} Y & 0 & 0 & 0 \\ 0 & Y & 0 & 0 \\ 0 & 0 & Y & 0 \\ 0 & 0 & 0 & Y \end{bmatrix}, \tag{43}$$

with $D^{(1)}_{ii} = \lambda^{K^L}_{n(i)}|_{R=b}$, $D^{(2)}_{ii} = \lambda^{V^L}_{n(i)}|_{R=b}$, $D^{(3)}_{ii} = \lambda^{K^L_{b,a}}_{n(i)}$, $D^{(4)}_{ii} = \lambda^{V^L_{b,a}}_{n(i)}$, $D^{(5)}_{ii} = \lambda^{K^L_{a,b}}_{n(i)}$, $D^{(6)}_{ii} = \lambda^{V^L_{a,b}}_{n(i)}$, $D^{(7)}_{ii} = \lambda^{K^L}_{n(i)}|_{R=a}$, $D^{(8)}_{ii} = \lambda^{V^L}_{n(i)}|_{R=a}$, $D^{(9)}_{ii} = \lambda^{K^Y}_{n(i)}|_{R=a}$, and $D^{(10)}_{ii} = \lambda^{V^Y}_{n(i)}|_{R=a}$, where $n(i)$ denotes the degree associated with the ith

eigenmode. Expanded in the surface harmonics, the unknowns of Eq. 11 are written

$$\begin{bmatrix} \tilde{\phi}_b \\ \frac{\partial\tilde{\phi}_b}{\partial n} \\ \tilde{\phi}_a \\ \frac{\partial\tilde{\phi}_a}{\partial n} \end{bmatrix} = \begin{bmatrix} Y^\star & 0 & 0 & 0 \\ 0 & Y^\star & 0 & 0 \\ 0 & 0 & Y^\star & 0 \\ 0 & 0 & 0 & Y^\star \end{bmatrix} \begin{bmatrix} \phi_b \\ \frac{\partial\phi_b}{\partial n} \\ \phi_a \\ \frac{\partial\phi_a}{\partial n}, \end{bmatrix} \tag{44}$$

and projecting the right-hand side similarly, we obtain the surface-harmonic analogue to Kirkwood's result:

$$\begin{bmatrix} \frac{1}{2}I + D^{(1)} & -D^{(2)} & 0 & 0 \\ \frac{1}{2}I - D^{(1)} & \epsilon_{p,w}D^{(2)} & D^{(3)} & -D^{(4)} \\ -D^{(5)} & \epsilon_{p,w}D^{(6)} & \frac{1}{2}I + D^{(7)} & -D^{(8)} \\ 0 & 0 & \frac{1}{2}I - D^{(9)} & D^{(10)} \end{bmatrix} \begin{bmatrix} \tilde{\phi}_b \\ \frac{\partial\tilde{\phi}_b}{\partial n} \\ \tilde{\phi}_a \\ \frac{\partial\tilde{\phi}_a}{\partial n} \end{bmatrix} = \begin{bmatrix} Y^\star\varphi_{\text{mol}} \\ 0 \\ 0 \\ 0 \end{bmatrix}. \tag{45}$$

Note that this representation does *not* diagonalize the entire operator, but does decompose the reaction potential in the protein into the individual harmonics.

An algorithm to solve the Kirkwood problem using the BIE/eigenfunction approach is therefore structured as follows. For each mode i to be solved (up to a desired order), one first computes the projection of the solute charge distribution onto the ith solid spherical harmonic (i.e. one computes the appropriate multipole expansion coefficient). Then one calculates the ith eigenvalues for the boundary integral operators to set up a linear system of equations with four unknowns, and solves for the ith expansion coefficient of the reaction potential. The reaction potentials at all desired locations is then easily computed. Explicit expressions are given in Appendix B.

3.2 Application to Nonlocal Electrostatics

We now derive our main result—the exact analytical solution of nonlocal electrostatics for a spherical solute. The 3-by-3 block operator of Eq. 29 can be decomposed as

$$\begin{bmatrix} Y & 0 & 0 \\ 0 & Y & 0 \\ 0 & 0 & Y \end{bmatrix} \begin{bmatrix} D^{(1)} & D^{(2)} & D^{(3)} \\ D^{(4)} & D^{(5)} & 0 \\ 0 & D^{(6)} & D^{(7)} \end{bmatrix} \begin{bmatrix} Y^\star & 0 & 0 \\ 0 & Y^\star & 0 \\ 0 & 0 & Y^\star \end{bmatrix}, \tag{46}$$

where again $Y^\star$ projects from a distribution on the sphere surface into an expansion in surface spherical harmonics, Y represents the harmonics themselves, and the matrices $D^{(k)}$ are all diagonal. The entries of the $D^{(k)}$ matrices are simply the appropriate scaled sum of the operator eigenvalues. Denoting the degree associated with the ith eigenmode by $n(i)$,

$$D^{(1)}_{ii} = \frac{1}{2} - \lambda^{K^Y_\Lambda}_{n(i)} \tag{47}$$

$$D^{(2)}_{ii} = -\frac{\epsilon_{\text{protein}}}{\epsilon_\infty}\lambda^{V^Y_\Lambda}_{n(i)} - \frac{\epsilon_{\text{protein}}}{\epsilon_{\text{water}}}\lambda^{V^{DR}_\Lambda}_{n(i)} \tag{48}$$

$$D^{(3)}_{ii} = \frac{\epsilon_\infty}{\epsilon_{\text{water}}}\lambda^{K^{DR}_\Lambda}_{n(i)} \tag{49}$$

$$D^{(4)}_{ii} = \frac{1}{2} + \lambda^{K^L}_{n(i)} \tag{50}$$

$$D^{(5)}_{ii} = -\lambda^{V^L}_{n(i)} \tag{51}$$

$$D^{(6)}_{ii} = \frac{\epsilon_{\text{protein}}}{\epsilon_\infty}\lambda^{V^L}_{n(i)} \tag{52}$$

$$D^{(7)}_{ii} = \frac{1}{2} - \lambda^{K^L}_{n(i)}. \tag{53}$$

Projecting both sides of Eq. 29, one obtains

$$\begin{bmatrix} D^{(1)} & D^{(2)} & D^{(3)} \\ D^{(4)} & D^{(5)} & 0 \\ 0 & D^{(6)} & D^{(7)} \end{bmatrix} \begin{bmatrix} \tilde{\varphi}_{\text{II}} \\ \frac{\partial\tilde{\varphi}_{\text{II}}}{\partial n} \\ \tilde{\Psi} \end{bmatrix} = \begin{bmatrix} \tilde{\xi} \\ 0 \\ 0 \end{bmatrix}, \tag{54}$$

where the ith entry of the projected form of Eq. 28 is defined by

$$\tilde{\xi}_i = -\left(\frac{1}{2} - \lambda^{K_A^Y}_{n(i)} + \frac{\epsilon_{\text{protein}}}{\epsilon_{\text{water}}}\lambda^{K_A^{DR}}_{n(i)}\right)\tilde{\varphi}_{\text{mol}} - \left(\frac{\epsilon_{\text{protein}}}{\epsilon_\infty}\lambda^{V_A^Y}_{n(i)} - \frac{\epsilon_{\text{protein}}}{\epsilon_{\text{water}}}\lambda^{V_A^{DR}}_{n(i)}\right)\frac{\partial\tilde{\varphi}_{\text{mol}}}{\partial n}. \tag{55}$$

Again, solving analytically for each coefficient $\tilde{\varphi}_{n(i)}$ independently provides the desired expansion (in surface harmonics) of the potential at the protein-water boundary. These coefficients are readily converted to the solid harmonics to obtain the potential inside the sphere. The analytical nonlocal model has been implemented in MATLAB and is available online [44], while explicit expressions are provided in Appendix B.

It may be verified that in the limits $\lambda \to 0$ and $\lambda \to \infty$, the analytical solution converges to the appropriate local-response models; see Figure 2 for the example of a sphere with a single central charge, which is known as the Born ion. As a more challenging validation, we have used the nlFFTSVD fast BEM solver [36] to compute the solvation free energy of a single $+1e$ charge situated at (0, 0, 6 Å) inside a sphere of radius 8 Å centered at the origin, and plotted the convergence of these results to the solvation free energy computed analytically (Figure 3). This test case is challenging because it lacks the spherical symmetry of the Born-ion test case, and in fact BEM simulations require finer discretization for charges close to the surface [39].

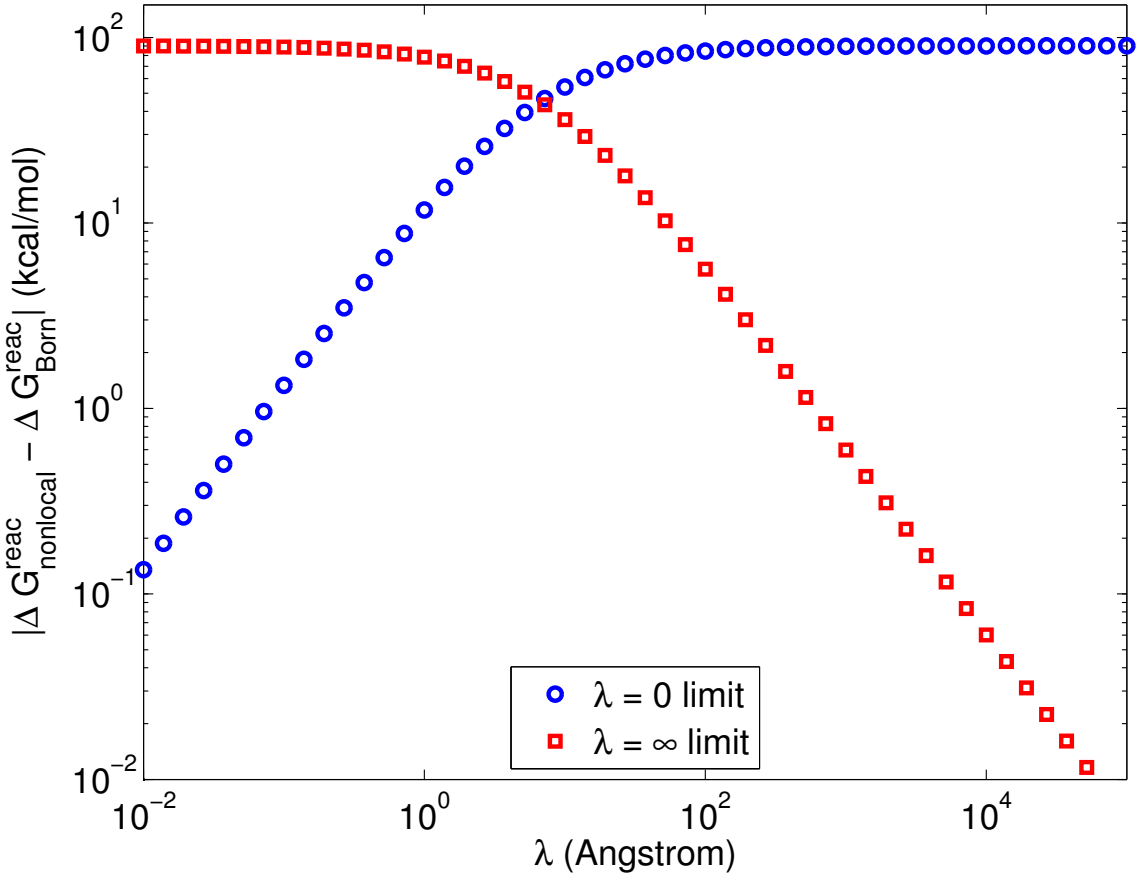

Figure 2: The analytically computed solvation free energy for a sphere with central charge (Born ion) converges to the correct local-response limits as the nonlocal length-scale parameter λ approaches 0 or ∞.

The required spherical Bessel and Hankel functions have been computed using the algorithm proposed by Cai [45], and their derivatives were calculated using well-known recurrence relations [46]. Using numerically stable implementations of the Bessel functions and their derivatives is of utmost importance. Most available implementations of these special functions do not provide accurate results for purely imaginary arguments (see Eq. 34), resulting in divergence of the solvation free energy as the order of the calculation

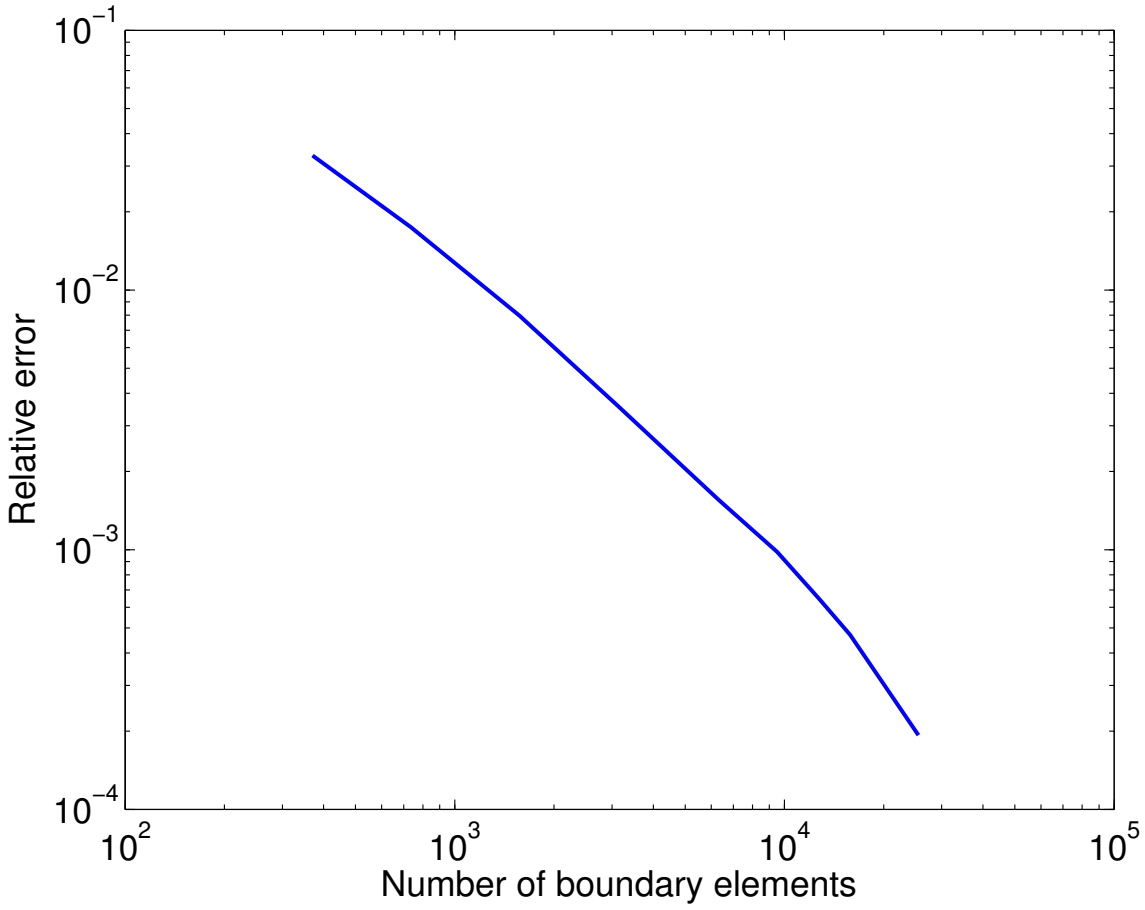

Figure 3: Relative error for numerical simulations of the nonlocal model using BEM, as a function of the number of unknowns in the discretized problem, for a 8-Å-radius sphere with a single $+1e$ charge situated 2 Å from the sphere surface.

is increased; very large and very small values of R/λ are particularly problematic for the calculation of the Yukawa-operator eigenvalues using standard methods. However, Vioreanu and Rokhlin have developed a much more accurate algorithm that promises to resolve these problems (personal communication).

4 Results

As a first application of the eigenfunction-expansion approach, we estimate the length scale parameter λ by comparison to both experiment and simulation. This application highlights that this particularly simple nonlocal model does not fully capture asymmetric dielectric response [47], and that improvements will be needed. Our second application illustrates that local and nonlocal models predict qualitatively different electrostatic fields at long length scales, offering important opportunities to establish the importance of nonlocality.

4.1 Reasonable λ

Early work on nonlocal models, by Kornyshev et al. (e.g. [48]) and by Basilevsky and Parsons [20], employed physically reasonable values of the length-scale parameter λ between 3 and 6 Angstroms, i.e. on the order of the size of a water molecule or two. More recent work on nonlocal models have employed much larger values; Hildebrandt *et al.* found $\lambda \approx 15 - 24$ Å provided an excellent fit to experimental data for monatomic

cations [17, 25], and others have used similarly large values [49]. We show here that two factors suffice to explain why recent work has needed such large λ, and properly accounting for these factors leads one to find the earlier range $\lambda = 4 - 6$ Å as optimal.

The first factor is the approach to parameterization; if one starts by assigning ions radii that are too small, then the solvation free energy will be large and a large λ will be needed to reduce it. Recalling that in these continuum models, the ion radius is the solute–solvent dielectric boundary, it seems reasonable to estimate the ion radius according to where the overall solvent charge distribution in MD simulations rises from zero [50]. Radii estimated in this manner are substantially larger than those employed in works that needed such large λ.

The second factor is the influence of the solvent structure around uncharged solutes, which is one reason why positive and negative charges have different solvation free energies [47]. In our recent study of ion solvation using molecular dynamics, we found that in an uncharged quasi-spherical solute representing a small molecule, the electrostatic potential due to solvent structure was on the order of 10 kcal/mol/e [51]; Ashbaugh has shown that this potential depends non-monotonically on the ion radius for small ions [52], though the magnitude of variation is small compared to the overall magnitude. This "static potential" contributes linearly to the electrostatic solvation free energy, so that instead of the usual linear-response model in which $\Delta G^{solv}(q) = \frac{1}{2} q^T L q$ where L is the usual reaction-potential operator, we have instead an affine-response model $\Delta G^{solv}(q) = \frac{1}{2} q^T L q + \phi^{\text{static},T} q$. Therefore, for monovalent cations and anions, the static potential contributes an asymmetry of $2e\phi^{\text{static}}$, or approximately 20 kcal/mol.

Figure 4 contains four plots that illustrate the influence of nonlocal response and the static potential. The solvation free energies in the upper plots ((a) and (b)) correspond to monovalent cations; those in the lower plots (c) and (d), to monovalent anions. The free energies in the left-hand side plots, (a) and (c), do not include the static-potential contribution, whereas those on the right-hand side, (b) and (d), do. The horizontal lines indicate Rashin and Honig's estimates of individual ion solvation free energies, which were derived from experimental measurements of salts [53]. The symbols represent Joung and Cheatham's ion radii (the Lennard-Jones $R_{min}/2$) from their thorough MD parameterization study of monovalent ions with multiple water models [54]; the red circles correspond to ion radii and solvation free energies in TIP3P water [55], and the blue squares are for SPC/E water [56] (Fedorov and Kornyshev have also used SPC/E water, to demonstrate the successes and limitations of nonlocal theory [56]).

Figure 4(a) illustrates that large λ, larger than 10 Å, are needed to fit experimental data, if one does not employ the static potential. Once the static potential is taken into account, however, as in Fig. 4(b), λ between 4 and 6 Å is quite satisfactory to predict cation solvation free energies if one merely uses standard Lennard-Jones radii. The discrepancy for the smallest ion, Li^+, is due in part to nonlinear response involving dielectric saturation, e.g. [57]. The story for anions is more complicated [47, 51, 58–60]. In Fig. 4(c) it seems that using Lennard-Jones radii leads to grossly *underestimated* electrostatic solvation free energies, even for the local-dielectric model, and that nonlocal response leads to even worse accuracy. Inclusion of the static-potential term (Fig. 4(d)) improves the situation significantly, but by no means completely.

These results are less unsatisfactory than they appear at first. Free-energy perturbation (FEP) calculations in explicit solvent show that for small ions, the electrostatic potential varies with a *piecewise linear* dependence on the ion charge, with one coefficient of linearity for positive charges and another coefficient for negative charges [51]. For an ion with the chloride anion Lennard-Jones parameters, the difference in these coefficients is approximately 18 kcal/mol/e^2 (the coefficients are -65.7 and -84.1 kcal/mol/e^2 for positive and negative charges), or about 27%. Scaling the local- and nonlocal-response coefficients for chloride using the Joung and Cheatham SPC/E radius of 2.711 Å, one obtains predicted solvation free energies of -99.5 kcal/mol for the local model, -91.9 kcal/mol for $\lambda = 4$ Å, and -89.0 kcal/mol when $\lambda = 6$ Å. These are surprisingly close to Rashin and Honig's estimate of -85.3 kcal/mol, and we note also these employ the same static potential term as used in the Figure, 10 kcal/mol/e, which is only approximate. Because the relative deviation in response coefficients varies as a function of the charge's proximity to solvent [51], this simple scaling cannot be applied immediately to the other ions in this series, which have different radii. However, the dramatic improvement from the predictions without the static potential, to including both the static potential and the water-steric components of asymmetry, provides extra support to the idea that small λ are appropriate.

Strictly speaking, of course, asymmetry constitutes nonlinear response, but one must be clear about what "response" is of interest. Fedorov and Kornyshev discuss nonlinear response in terms of the screening factor, which is a function of position and proportional to the electrostatic potential *in the solvent* [47]. This function is not only nonlinear, but very complicated (see Figure 5 in [47]). For many applications of implicit-solvent models, however, one cares only about the potential in the *solute*. As shown in our earlier work [51], even for small ions, the potential appears to change piecewise linearly with the charge distribution, which is a comparatively simple nonlinearity. It is possible that capturing this effect will still require the full sophistication of nonlocal models tested by Kornyshev et al., but perhaps simplifications of their advanced theories will be found.

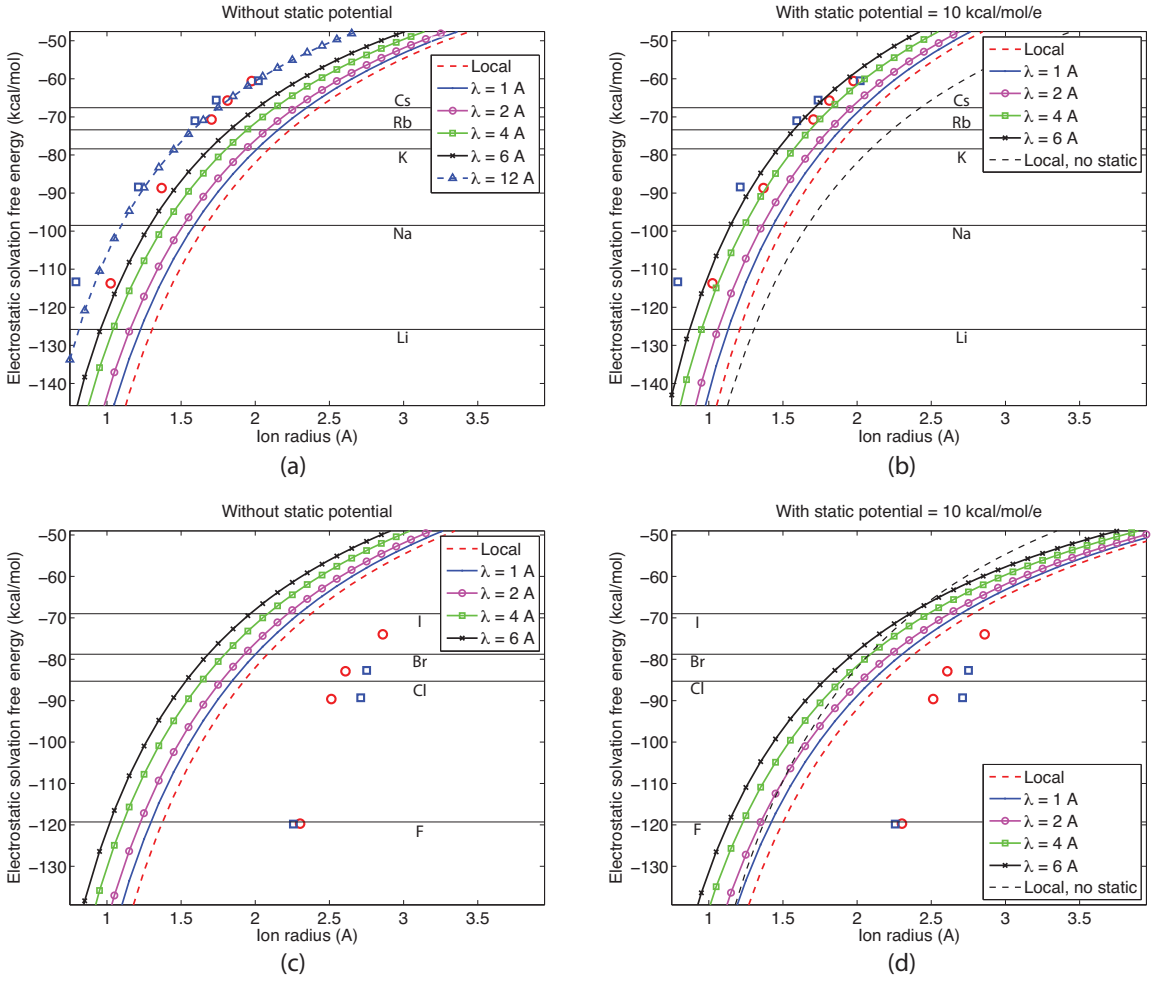

Figure 4: Electrostatic solvation free energies for monovalent ions of varying radii for local and nonlocal electrostatic models, when one either omits the energetic contribution induced by solvent structure for an uncharged solute (the static potential [51]), as shown in the plots on the left, or includes its contribution, as shown in the plots on the right. The horizontal lines represent Rashin and Honig's estimates from experimental measurements on salts [53]; the symbols represent Joung and Cheatham's optimized Lennard-Jones radii ($R_{min}/2$) for TIP3P water (red circles) and SPC/E water (blue squares) [54]. The static potential is set to 10 kcal/mol/e for all radii, which is an approximation [52]. (a) Cation solvation free energies calculated without the static potential; (b) Cation solvation free energies calculated with the static potential; (c) Anion solvation free energies calculated without the static potential; (d) Anion solvation free energies calculated with the static potential. In these calculations, $\epsilon_{\text{protein}} = 1$, $\epsilon_{\text{water}} = 80$, and $\epsilon_{\infty} = 1.8$.

4.2 Spherical Models of Proteins

Analytical solutions for simple geometries also allow fast determination of the reaction potential throughout the whole system. More thorough visualizations of solvent response may offer new insights into the empirical, seemingly application-specific definitions of the protein dielectric constant [61, 62], including for example why values of $\epsilon_{\text{protein}}$ much larger than experimental estimates [63] are often needed to obtain accurate calculations of pK_a shifts in proteins [64]. To illustrate the fundamental differences between local and nonlocal theory, as well as the computational advantage of having a fast analytical model for visualization, we plot the reaction potentials for both simple and complicated charge distributions as we vary key model parameters: the protein dielectric constant in the local theory, and the effective length scale λ in the nonlocal model.

Figure 5 contains plots of the reaction potential induced by a single $+1e$ charge in a protein-sized sphere of radius 24 Å, where the charge is situated 2 Å from the dielectric boundary. The reaction potential for local-response models is shown in (a) and (b), with $\epsilon_{\text{protein}} = 2$ in (a) and $\epsilon_{\text{protein}} = 4$ in (b). Nonlocal-model results are plotted in (c) and (d); for both nonlocal calculations, $\epsilon_{\text{protein}} = 2$, with $\lambda = 1$ Å in (c) and $\lambda = 5$ Å in (d). For comparison, all potentials are plotted according to the same color scale. Adjusting $\epsilon_{\text{protein}}$ from 2 to 4 in the local model leads to a qualitative global shift in the reaction potential. On the other hand, nonlocal response presents relatively small overall changes, even though λ varies substantially. For a single $+1e$ charge buried deep within the protein at (0, 0, 10 Å), the reaction potential is smaller in magnitude, which means that the qualitative shift for increased $\epsilon_{\text{protein}}$ can be seen more easily (Figure 6).

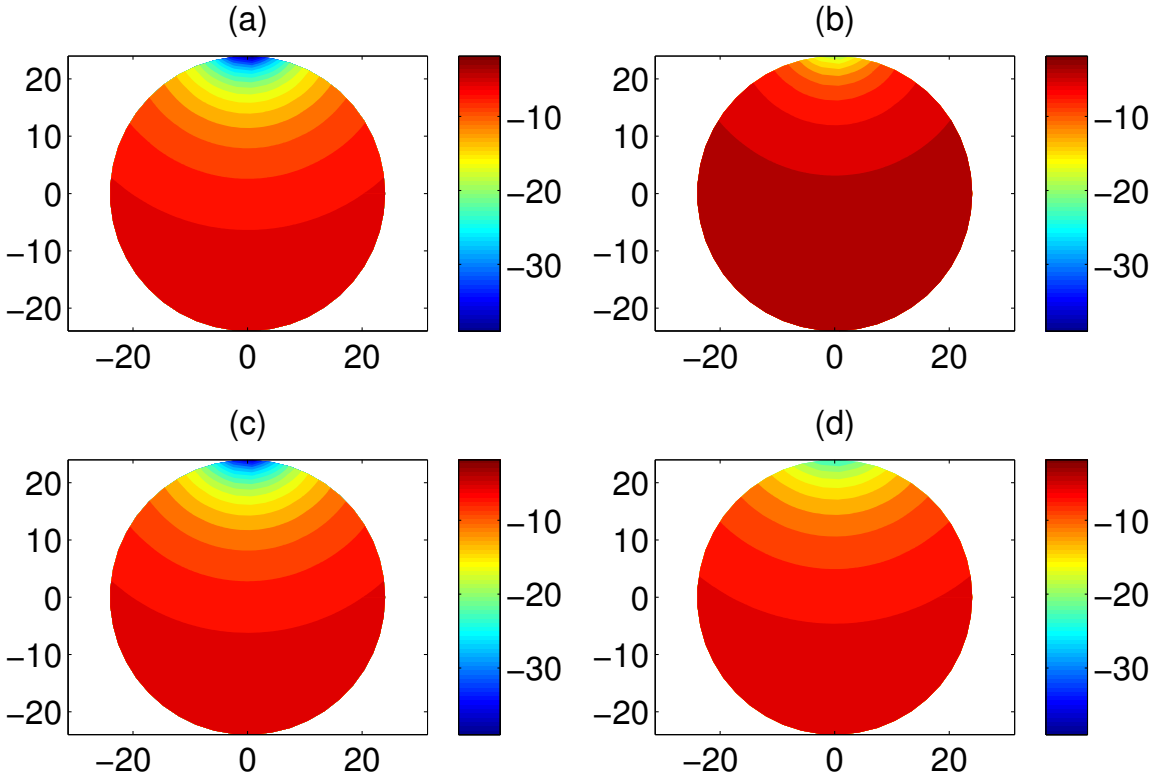

Figure 5: Reaction potential (in kcal/mol/e) induced in a sphere of radius 24 Å by a single $+1e$ point charge situated 2 Å from the boundary, for different local and nonlocal models. All potentials are plotted on the same color scale, and for all models, $\epsilon_{\text{water}} = 80$. (a) Local-response model with $\epsilon_{\text{protein}} = 2$; (b) local-response model with $\epsilon_{\text{protein}} = 4$; (c) nonlocal-response model with $\epsilon_{\text{protein}} = 2$ and $\lambda = 1$ Å; (d) nonlocal-response model with $\epsilon_{\text{protein}} = 2$ and $\lambda = 10$ Å.

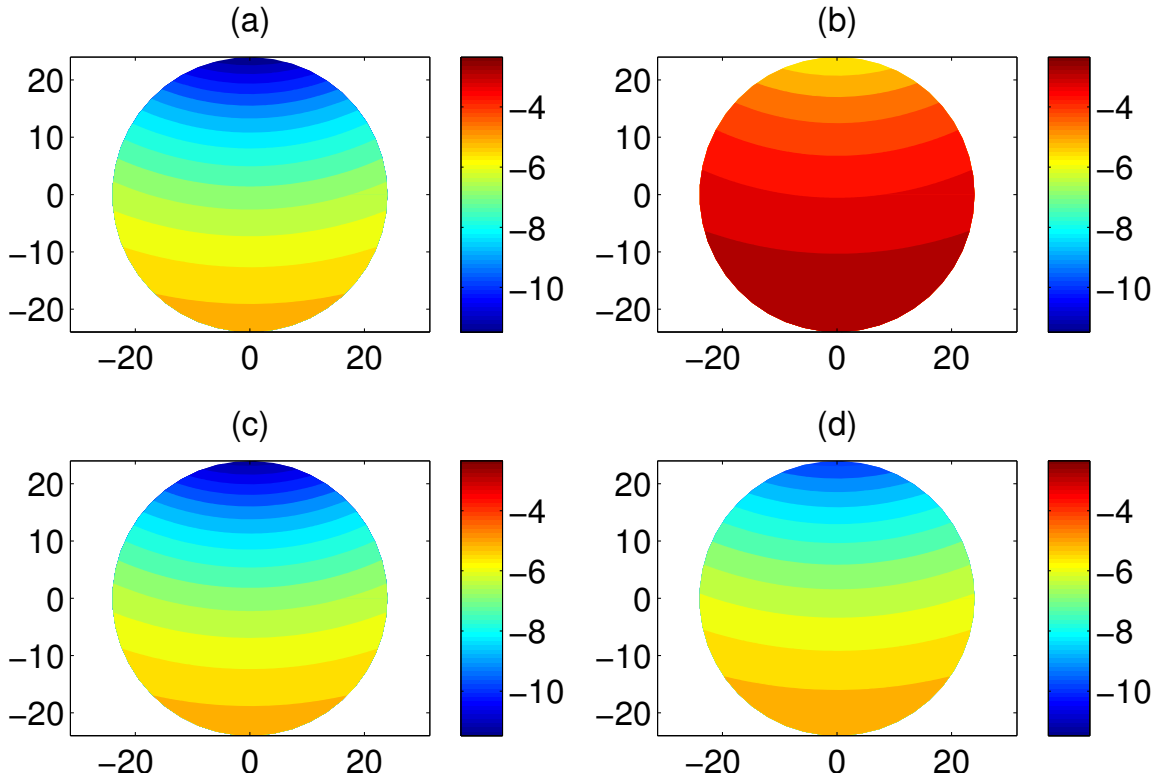

Figure 6: Reaction potential (in kcal/mol/e) induced in a sphere of radius 24 Å by a single $+1e$ point charge buried 14 Å from the boundary, for different local and nonlocal models. All model parameters are the same as the corresponding plots in Figure 5.

4.3 Computational Efficiency

We would like to emphasize the substantial difference in speed between numerical and analytical methods. For calculating the reaction-potential operator on a test problem involving a sphere of radius 24 Å, with 500 charges inside, a low-resolution numerical simulation using the highly optimized, linear-scaling boundary-element method (BEM) code nlFFTSVD [36]—one of the fastest numerical implementations of the nonlocal model—requires approximately 25 minutes on a 2012 MacBook Air, and 540 megabytes (MB) of memory. In contrast, the unoptimized MATLAB implementation of the eigenfunction-expansion approach (i.e. the MATLAB code is interpreted rather than compiled) requires less than 7 seconds on the same computer, making it about 200 times faster, and it requires only about 1 MB of memory. As shown in Figure 7, the effect of nonlocality is the same in realistic charge distributions as for simple model ones—nonlocality permits surface charge solvation to be strongly modulated, as if by smaller dielectric contrast between solute and solvent, while buried charges still essentially see the "standard" high dielectric contrast. On the other hand, the common practice of changing the solute dielectric constant affects both types of charges drastically (Figure 7(b)).

5 Discussion

The shortcomings of local electrostatics continue to motivate new models, but often the practical complications of numerical simulation slow their testing and improvement. To accelerate studies of the promising Lorentz nonlocal model [17, 26, 27, 65], we have derived the exact analytical solution for a spherical solute containing an arbitrary charge distribution. Our approach uses Hildebrandt's boundary-integral equation (BIE) formulation [26] and the analytically known eigendecompositions of the associated boundary-integral

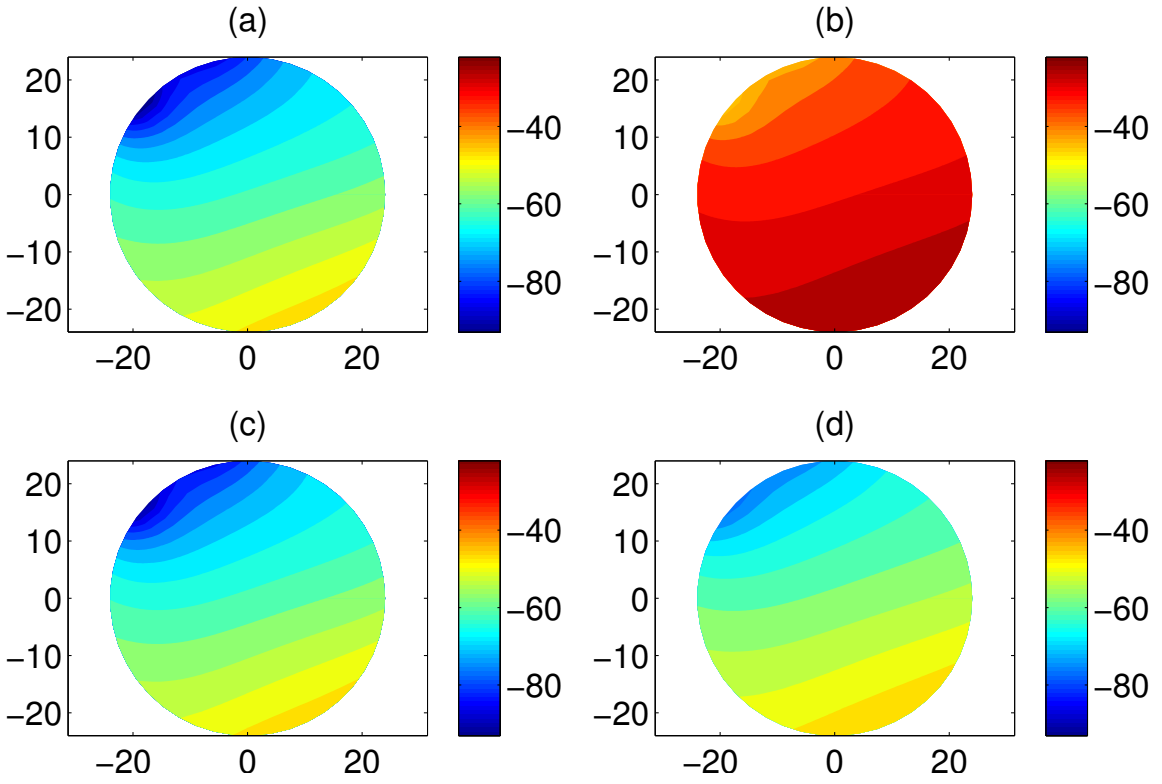

Figure 7: Reaction potential (in kcal/mol/e) induced in a sphere of radius 24 Å by the charge distribution of the protein bovine pancreatic trypsin inhibitor (BPTI), for different local and nonlocal models. All model parameters are the same as the corresponding plots in Figure 5. See main text for full computational details.

operators. Calculations demonstrate the method's correctness and that solvent screening of charge-charge interactions are markedly different in nonlocal and local theories, even when the protein dielectric constant is adjusted. Fast analytical models enable rapid visualization of electrostatic fields, and thus facilitates efficient exploration of the new model's implications and qualitative differences from existing theories. The BIE-eigenfunction strategy represents a novel alternative to matching potential expansions and may be useful in other areas of mathematical physics. To illustrate the method's generality, we have also derived the solution to the Kirkwood two-boundary problem for local electrostatics, which has furnished many insightful physical studies and model approximations even though proteins clearly take shapes much more complex than spheres.

The present work enables studies of the nonlocal model to be conducted rapidly for simple model systems, obviating the need for more complicated and slower numerical calculations [26, 27, 36, 65]. To encourage further tests of nonlocal models, we have made freely available our MATLAB implementation of the analytical approach [44]. As described in earlier work on nonlocal electrostatics, boundary conditions represent a subtle issue that warrants detailed study [25, 27, 31], and fast calculations on spheres will allow a simple way to test improvements. Our results also provide a useful way to test numerical simulations of nonlocal electrostatics on nontrivial systems, e.g. models of finite-sized solutes with complicated charge distributions.

Future work will address the development of fast analytical approximations similar to recent Generalized-Born (GB) models [9] or BIE approximations [66]. Second-kind boundary-integral formulations may offer substantial advantages for such approximations [67], and Fasel et al. have recently presented a purely second-kind formulation of the nonlocal model [31]. An extension of our approach to the Fasel formulation is therefore of significant interest. One extension to the present work might be to account for the fact that many proteins can be reasonably well modeled using ellipsoids (see, for a recent example in electrostatic theory, [68]). It is possible that one could use a similar approach to derive an analytical solution for ellipsoidal geometries as

well; the eigendecompositions of the Laplace boundary-integral operators for ellipsoids are known, for instance [13, 69, 70], though corresponding results for the Yukawa integral operators do not appear to have been published. We also note that even for the sphere, computing the eigenvalues of the Yukawa integral operators is numerically challenging, and should motivate the development of improved algorithms. Recent work on computing the ellipsoidal harmonics found similar challenges [71], and the present work has uncovered a second compelling example of how molecular biophysics poses novel challenges for more fundamental research in applied mathematics and numerical analysis.

Appendix A: Eigenvalues of the Laplace boundary-integral operators for concentric spheres

We first address the single- and double-layer operators that map from the inner sphere (radius b) to the outer (radius a). For the single-layer operator, let us expand a surface potential on the inner sphere in surface harmonics, i.e.

$$\psi_{S_b} = \sum_{n,m} S^b_{nm} Y^m_n(\theta, \phi). \tag{56}$$

and also expand the potential field in the region outside that sphere

$$\psi = \sum_{n,m} V_{nm} r^{-(n+1)} Y^m_n(\theta, \phi). \tag{57}$$

These two fields must agree on the surface $r = b$, and by orthogonality of the Y^m_n functions, we have

$$V_{nm} = S^b_{nm} b^{n+1}. \tag{58}$$

A similar surface expansion holds for the fields on the outer concentric sphere

$$\psi_{S_a} = \sum_{n,m} S^a_{nm} Y^m_n(\theta, \phi), \tag{59}$$

which may be matched to Eq. 57 to give

$$V_{nm} = a^{n+1} S^a_{nm}. \tag{60}$$

Combining Eq. 58 with Eq. 60, we have

$$S^a_{nm} = \frac{b^{n+1}}{a^{n+1}} S^b_{nm} \tag{61}$$

Because the eigenvalue for the single-layer Laplace surface operator on the inner surface is $b/(2n+1)$, we finally have that

$$\lambda_n^{V^L_{a,b}} = \left(\frac{b}{a}\right)^{n+1} \frac{b}{2n+1}. \tag{62}$$

We derive the double-layer potential operators using an alternative approach based on Green's theorem. Consider again the expansion in spherical harmonics of the potential outside b from Eq. 57, so that the radial component of the electric field is

$$\frac{\partial \psi}{\partial r} = \sum_{n,m} V_{nm}(-(n+1)) r^{-(n+2)} Y^m_n(\theta, \phi), \tag{63}$$

so the normal derivative of the potential at the inner surface b is

$$\frac{\partial \psi}{\partial r}|_{r=b} = \sum_{n,m} V_{nm}(-(n+1)) b^{-(n+2)} Y^m_n(\theta, \phi). \tag{64}$$

Green's theorem allows us to write the potential at any point $\mathbf{r}$ with $r = a > b$ as

$$\psi(\mathbf{r}) = + \int_b \frac{\partial G(\mathbf{r}, \mathbf{r}')}{\partial n} \psi(\mathbf{r}') dA' - \int_b G(\mathbf{r}, \mathbf{r}') \frac{\partial \psi(\mathbf{r}')}{\partial n} dA'. \tag{65}$$

Using Eq. 30 and again relying on the orthogonality of the harmonics, we obtain

$$a^{-(n+1)} = \lambda_n^{K^L_{a,b}} b^{-(n+1)} - \lambda_n^{V^L_{a,b}}(-(n+1))b^{-(n+2)}; \tag{66}$$

substituting the known $\lambda_n^{V^L_{a,b}}$ from Eq. 62 gives

$$a^{-(n+1)} = \lambda_n^{K^L} b^{-(n+1)} + \frac{n+1}{2n+1} a^{-(n+1)} \tag{67}$$

and finally

$$\lambda_n^{K^L} = \frac{n}{2n+1}\left(\frac{b}{a}\right)^{n+1}. \tag{68}$$

This result may be checked in the limit as $a \to b$, where Eq. 65 becomes

$$\psi(\mathbf{r}) = \frac{1}{2}\psi(\mathbf{r}) + \int \frac{\partial G(\mathbf{r},\mathbf{r}')}{\partial n}\psi(\mathbf{r}')dA' - \int G(\mathbf{r},\mathbf{r}')\frac{\partial \psi(\mathbf{r}')}{\partial n}dA'. \tag{69}$$

Analogous manipulations lead to the relation

$$a^{-(n+1)} = \frac{1}{2}a^{-(n+1)} + \lambda_{nm}^K b^{-(n+1)} + \frac{n+1}{2n+1}a^{-(n+1)} \tag{70}$$

and thus we recover the self-surface result that $\lambda_n^{K^L} = \frac{-1}{2(2n+1)}$. The eigenvalues for the operators that map from the outer sphere to the inner one are obtained in very similar fashion using interior harmonics. For example,

$$\psi = \sum_{n,m} V_{nm} r^n Y_n^m(\theta,\phi), \tag{71}$$

and equating coefficients as before

$$V_{nm} = \frac{1}{a^n} S_{nm}^a = \frac{1}{b^n} S_{nm}^a \tag{72}$$

so that we have for the single-layer

$$\lambda_n^{V^L_{b,a}} = \left(\frac{a}{b}\right)^n \frac{a}{2n+1}. \tag{73}$$

The eigenvalues presented for these operators can be verified analytically using Green's theorem.

Appendix B: Explicit expressions for modal coefficients

Returning to (45), we can write the matrix in a simplified form

$$\left[\begin{array}{cc|cc} a & b & 0 & 0 \\ c & d & e & f \\ \hline g & h & i & j \\ 0 & 0 & k & l \end{array}\right] \tag{74}$$

which has inverse

$$\frac{1}{\Delta}\left[\begin{array}{cc|cc} fhk - djk - ehl + dil & bjk - bil & bel - bfk & bfi - bej \\ -fgk + cjk + egl - cil & ail - ajk & afk - ael & aej - afi \\ \hline chl - dgl & bgl - ahl & adl - bcl & -bfg + afh + bcj - adj \\ dgk - chk & ahk - bgk & bck - adk & beg - aeh - bci + adi \end{array}\right] \tag{75}$$

where

$$\Delta = a(dil - djk - ehl + fhk) + b(-cil + cjk + egl - fgk). \tag{76}$$

This can be multiplied by the original matrix to verify that it is indeed the inverse. Since the RHS in (45) has a single nonzero component, our solution is given by

$$\frac{\tilde{\phi}_{mol}}{\Delta}\begin{bmatrix} fhk - djk - ehl + dil \\ -fgk + cjk + egl - cil \\ chl - dgl \\ dgk - chk \end{bmatrix} \tag{77}$$

Plugging in the definitions from Sec. 3.1, we have

$$\begin{aligned}
\tilde{\phi}_b^i &= \frac{\tilde{\phi}_{mol}}{\Delta_i}\Big(-\lambda_{n(i)}^{V_{b,a}^L}\epsilon_{I,II}\lambda_{n(i)}^{V_{a,b}^L}(1/2-\lambda_{n(i)}^{K^Y}|_{R=a}) - \epsilon_{I,II}\lambda_{n(i)}^{V^L}|_{R=b}\lambda_{n(i)}^{V^L}|_{R=a}(1/2-\lambda_{n(i)}^{K^Y}|_{R=a}) \\
&\quad - \lambda_{n(i)}^{K_{b,a}^L}\epsilon_{I,II}\lambda_{n(i)}^{V_{a,b}^L}\lambda_{n(i)}^{V^Y}|_{R=a} - \epsilon_{I,II}\lambda_{n(i)}^{V^L}|_{R=b}(1/2+\lambda_{n(i)}^{K^L}|_{R=a})\lambda_{n(i)}^{V^Y}|_{R=a}\Big) \\
\frac{\partial\tilde{\phi}_b^i}{\partial n} &= \frac{\tilde{\phi}_{mol}}{\Delta_i}\Big(-\lambda_{n(i)}^{V_{b,a}^L}\lambda_{n(i)}^{K_{a,b}^L}(1/2-\lambda_{n(i)}^{K^Y}|_{R=a}) - (1/2-\lambda_{n(i)}^{K^L}|_{R=b})\lambda_{n(i)}^{V^L}|_{R=a}(1/2-\lambda_{n(i)}^{K^Y}|_{R=a}) \\
&\quad - \lambda_{n(i)}^{K_{b,a}^L}\lambda_{n(i)}^{K_{a,b}^L}\lambda_{n(i)}^{V^Y}|_{R=a} - (1/2-\lambda_{n(i)}^{K^L}|_{R=b})(1/2+\lambda_{n(i)}^{K^L}|_{R=a})\lambda_{n(i)}^{V^Y}|_{R=a}\Big) \\
\tilde{\phi}_a^i &= \frac{\tilde{\phi}_{mol}}{\Delta_i}\Big((1/2-\lambda_{n(i)}^{K^L}|_{R=b})\epsilon_{I,II}\lambda_{n(i)}^{V_{a,b}^L}\lambda_{n(i)}^{V^Y}|_{R=a} + \epsilon_{I,II}\lambda_{n(i)}^{V^L}|_{R=b}\lambda_{n(i)}^{K_{a,b}^L}\lambda_{n(i)}^{V^Y}|_{R=a}\Big) \\
\frac{\partial\tilde{\phi}_a^i}{\partial n} &= \frac{\tilde{\phi}_{mol}}{\Delta_i}\Big(-\epsilon_{I,II}\lambda_{n(i)}^{V^L}|_{R=b}\lambda_{n(i)}^{K_{a,b}^L}(1/2-\lambda_{n(i)}^{K^Y}|_{R=a}) - (1/2-\lambda_{n(i)}^{K^L}|_{R=b})\epsilon_{I,II}\lambda_{n(i)}^{V_{a,b}^L}(1/2-\lambda_{n(i)}^{K^Y}|_{R=a})\Big)
\end{aligned}$$

where

$$\begin{aligned}
\Delta_i &= (1/2+\lambda_{n(i)}^{K^L}|_{R=b})\Big(\epsilon_{I,II}\lambda_{n(i)}^{V^L}|_{R=b}(1/2+\lambda_{n(i)}^{K^L}|_{R=a})\lambda_{n(i)}^{V^Y}|_{R=a} + \epsilon_{I,II}\lambda_{n(i)}^{V^L}|_{R=b}\lambda_{n(i)}^{V^L}|_{R=a}(1/2-\lambda_{n(i)}^{K^Y}|_{R=a}) \\
&\quad - \lambda_{n(i)}^{K_{b,a}^L}\epsilon_{I,II}\lambda_{n(i)}^{V_{a,b}^L}\lambda_{n(i)}^{V^Y}|_{R=a} - \lambda_{n(i)}^{V_{b,a}^L}\epsilon_{I,II}\lambda_{n(i)}^{V_{a,b}^L}(1/2-\lambda_{n(i)}^{K^Y}|_{R=a})\Big) - \lambda_{n(i)}^{V^L}|_{R=b}\Big(-(1/2-\lambda_{n(i)}^{K^L}|_{R=b})(1/2+\lambda_{n(i)}^{K^L}|_{R=a})\lambda_{n(i)}^{V^Y}|_{R=a} \\
&\quad - (1/2-\lambda_{n(i)}^{K^L}|_{R=b})\lambda_{n(i)}^{V^L}|_{R=a}(1/2-\lambda_{n(i)}^{K^Y}|_{R=a}) - \lambda_{n(i)}^{K_{b,a}^L}\lambda_{n(i)}^{K_{a,b}^L}\lambda_{n(i)}^{V^Y}|_{R=a} - \lambda_{n(i)}^{V_{b,a}^L}\lambda_{n(i)}^{K_{a,b}^L}(1/2-\lambda_{n(i)}^{K^Y}|_{R=a})\Big).
\end{aligned}$$

In the case of nonlocal electrostatics, (54), we have

$$\begin{bmatrix} a & b & c \\ d & e & 0 \\ 0 & f & g \end{bmatrix} \tag{78}$$

which has inverse

$$\frac{1}{\Delta}\begin{bmatrix} eg & cf-bg & -ce \\ -dg & ag & cd \\ df & -af & ae-bd \end{bmatrix} \tag{79}$$

where

$$\Delta = aeg - bdg + cdf. \tag{80}$$

Plugging in the definitions from Sec. 3.2, we have

$$\begin{aligned}
\tilde{\phi}_{II}^i &= \frac{\tilde{\xi}_i}{\Delta_i}\left(-\lambda_{n(i)}^{V^L}\left(\frac{1}{2}-\lambda_{n(i)}^{K^L}\right)\right) \\
\frac{\partial\tilde{\phi}_{II}^i}{\partial n} &= \frac{\tilde{\xi}_i}{\Delta_i}\left(-(\frac{1}{2}+\lambda_{n(i)}^{K^L})\left(\frac{1}{2}-\lambda_{n(i)}^{K^L}\right)\right) \\
\tilde{\Psi}^i &= \frac{\tilde{\xi}_i}{\Delta_i}\left(\left(\frac{1}{2}+\lambda_{n(i)}^{K^L}\right)\frac{\epsilon_{\text{protein}}}{\epsilon_\infty}\lambda_{n(i)}^{V^L}\right)
\end{aligned}$$

where

$$\Delta_i = -\left(\frac{1}{2} - \lambda^{K^Y_\Lambda}_{n(i)}\right)\lambda^{V^L}_{n(i)}\left(\frac{1}{2} - \lambda^{K^L}_{n(i)}\right) - \left(-\frac{\epsilon_{\text{protein}}}{\epsilon_\infty}\lambda^{V^Y_\Lambda}_{n(i)} - \frac{\epsilon_{\text{protein}}}{\epsilon_{\text{water}}}\lambda^{V^{DR}_\Lambda}_{n(i)}\right)\left(\frac{1}{2} + \lambda^{K^L}_{n(i)}\right)\left(\frac{1}{2} - \lambda^{K^L}_{n(i)}\right) + \frac{\epsilon_\infty}{\epsilon_{\text{water}}}\lambda^{K^{DR}_\Lambda}_{n(i)}\left(\frac{1}{2} + \lambda^{K^L}_{n(i)}\right)\frac{\epsilon_{\text{protein}}}{\epsilon_\infty}\lambda^{V^L}_{n(i)}$$

using the definition of $\tilde{\xi}_i$ from (55).

Acknowledgement: The work of JPB was supported in part by a New Investigator award from Rush University and by the National Institute Of General Medical Sciences (NIGMS) of the National Institutes of Health (NIH) under award number R21GM102642. The content is solely the responsibility of the authors and does not necessarily represent the official views of the National Institutes of Health. MGK acknowledges partial support from the Office of Advanced Scientific Computing Research, Office of Science, U.S. Department of Energy, under Contract DE-AC02-06CH11357 and the U.S. Army Research Laboratory and the U.S. Army Research Office under contract/grant number W911NF-09-0488. PRB acknowledges full support from U.S. DOE Contract DE-AC01-06CH11357. The authors gratefully acknowledge A. Hildebrandt for valuable discussions, R. S. Eisenberg for his ongoing support of their collaboration, and B. Vioreanu and V. Rokhlin for generously sharing their work on accurate calculations of special functions.

Conflict of interest: Authors state no conflict of interest.

References

[1] B. Roux and T. Simonson. Implicit solvent models. *Biophys. Chem.*, 78:1–20, 1999.
[2] C. Azuara, H. Orland, M. Bon, P. Koehl, and M. Delarue. Incorporating dipolar solvents with variable density in Poisson–Boltzmann electrostatics. *Biophys. J.*, 95:5587–5605, 2008.
[3] P. Koehl and M. Delarue. AQUASOL: an efficient solver for the dipolar Poisson–Boltzmann–Langevin equation. *J. Chem. Phys.*, 132:064101, 2010.
[4] J. G. Kirkwood. Theory of solutions of molecules containing widely separated charges with special application to zwitterions. *J. Chem. Phys.*, 2:351, 1934.
[5] J. D. Jackson. *Classical Electrodynamics*. Wiley, 3^{rd} edition, 1998.
[6] J. J. Havranek and P. B. Harbury. Tanford–Kirkwood electrostatics for protein modeling. *Proc. Natl. Acad. Sci. USA*, 96(20):11145–11150, 1999.
[7] H.-X. Zhou. Control of reduction potential by protein matrix: lesson from a spherical protein model. *Journal of Biological Inorganic Chemistry*, 2:109–113, 1997.
[8] E. Kangas and B. Tidor. Optimizing electrostatic affinity in ligand–receptor binding: Theory, computation, and ligand properties. *J. Chem. Phys.*, 109:7522–7545, 1998.
[9] G. Sigalov, P. Scheffel, and A. Onufriev. Incorporating variable dielectric environments into the generalized Born model. *J. Chem. Phys.*, 122:094511, 2005.
[10] I. M. Mladenov. Kirkwood's formula revisited. *Europhysics Letters*, 33:577–581, 1996.
[11] K. E. Atkinson. *The Numerical Solution of Integral Equations of the Second Kind*. Cambridge University Press, 1997.
[12] J. J. Bowman, T. B. A. Senior, and P. L. E. Uslenghi. *Electromagnetic and acoustic scattering by simple shapes*. North-Holland, Amsterdam, 1969.
[13] R. E. Kleinman, R. Kress, and E. Martensen, editors. *The spectrum of the electrostatic integral operator for an ellipsoid*, Frankfurt/Bern, 1995. Lang.
[14] R. R. Dogonadze and A. A. Kornyshev. Polar solvent structure in the theory of ionic solvation. *J. Chem. Soc. Faraday Trans. 2*, 70:1121–1132, 1974.
[15] A. A. Kornyshev, A. I. Rubinshtein, and M. A. Vorotyntsev. Model nonlocal electrostatics: I. *Journal of Physics C: Solid State Physics*, 11:3307, Dec 1978.
[16] M. V. Basilevsky and D. F. Parsons. An advanced continuum medium model for treating solvation effects: Nonlocal electrostatics with a cavity. *J. Chem. Phys.*, 105(9):3734, Aug 1996.
[17] A. Hildebrandt, R. Blossey, S. Rjasanow, O. Kohlbacher, and H.-P. Lenhof. Novel formulation of nonlocal electrostatics. *Phys. Rev. Lett.*, 93:108104, 2004.
[18] A. Rubinstein and S. Sherman. Influence of the solvent structure on the electrostatic interactions in proteins. *Biophys. J.*, 87(3):1544–1557, Sep 2004.

[19] P. Attard, D. Wei, and G. N. Patey. Critical comments on the nonlocal dielectric function employed in recent theories of the hydration force. *Chemical Physics Letters*, 172:69–72, 1990.
[20] M. V. Basilevsky and D. F. Parsons. Nonlocal continuum solvation model with exponential susceptibility kernels. *J. Chem. Phys.*, 108:9107–9113, 1998.
[21] S. Weggler. *Correlation induced electrostatic effects in biomolecular systems*. PhD thesis, Universität des Saarlandes, 2010.
[22] A. Rubinstein and S. Sherman. Evaluation of the influence of the internal aqueous solvent structure on electrostatic interactions at the protein-solvent interface by nonlocal continuum electrostatic approach. *Biopolymers*, 87(2-3):149–164, Oct 2007.
[23] A. Rubinstein, R. Sabirianov, W. Mei, F. Namavar, and A. Khoynezhad. Effect of the ordered interfacial water layer in protein complex formation: A nonlocal electrostatic approach. *Phys. Rev. E*, 82(2):021915, Aug 2010.
[24] M. A. Vorotyntsev. Model nonlocal electrostatics. II. spherical interface. *Journal of Physics C: Solid State Physics*, 11:3323–3331, 1978.
[25] A. Hildebrandt. *Biomolecules in a structured solvent: A novel formulation of nonlocal electrostatics and its numerical solution*. PhD thesis, Universität des Saarlandes, 2005.
[26] A. Hildebrandt, R. Blossey, S. Rjasanow, O. Kohlbacher, and H.-P. Lenhof. Electrostatic potentials of proteins in water: a structured continuum approach. *Bioinformatics*, 23(2):e99–e103, Jan 2007.
[27] S. Weggler, V. Rutka, and A. Hildebrandt. A new numerical method for nonlocal electrostatics in biomolecular simulations. *J. Comput. Phys.*, 229(11):4059–4074, Jun 2010.
[28] R. L. Ochs Jr. and G. Kristensson. Using local differential operators to model dispersion in dielectric media. *Journal of the optical society of America A*, 15:2208–2215, 1998.
[29] R. A. B. Engelen, M. G. D. Geers, and F. P. T. Baaijens. Nonlocal implicit gradient-enhanced elasto-plasticity for the modelling of softening behavior. *International Journal of Plasticity*, 19:403–433, 2003.
[30] J. P. Bardhan. Gradient models in molecular biophysics: progress, challenges, opportunities. *Journal of Mechanical Behavior of Materials*, 22:169–184, 2013.
[31] C. Fasel, S. Rjasanow, and O. Steinbach. A boundary integral formulation for nonlocal electrostatics. In Karl Kunisch, Günther Of, and Olaf Steinbach, editors, *Numerical Mathematics and Advanced Applications*, pages 117–124. Springer Berlin Heidelberg, 2008.
[32] N. A. Baker, D. Sept, M. J. Holst, and J. A. McCammon. Electrostatics of nanoysystems: Application to microtubules and the ribosome. *Proc. Natl. Acad. Sci. USA*, 98:10037–10041, 2001.
[33] A. H. Boschitsch, M. O. Fenley, and H.-X. Zhou. Fast boundary element method for the linear Poisson–Boltzmann equation. *J. Phys. Chem. B*, 106(10):2741–54, 2002.
[34] B. Z. Lu, X. L. Cheng, J. Huang, and J. A. McCammon. Order N algorithm for computation of electrostatic interactions in biomolecular systems. *Proc. Natl. Acad. Sci. USA*, 103(51):19314–19319, 2006.
[35] M. D. Altman, J. P. Bardhan, J. K. White, and B. Tidor. Accurate solution of multi-region continuum electrostatic problems using the linearized Poisson–Boltzmann equation and curved boundary elements. *J. Comput. Chem.*, 30:132–153, 2009.
[36] J. P. Bardhan and A. Hildebrandt. A fast solver for nonlocal electrostatic theory in biomolecular science and engineering. In *IEEE/ACM Design Automation Conference (DAC)*, 2011.
[37] J. Warwicker and H. C. Watson. Calculation of the electric potential in the active site cleft due to alpha-helix dipoles. *J. Mol. Biol.*, 157:671–679, 1982.
[38] D. Xie, Y. Jiang, and L. R. Scott. Efficient algorithms for a nonlocal dielectric model for protein in ionic solvent. *SIAM Journal of Scientific and Statistical Computing*, 35:B1267–B1284, 2013.
[39] A. H. Juffer, E. F. F. Botta, B. A. M. van Keulen, A. van der Ploeg, and H. J. C. Berendsen. The electric potential of a macromolecule in a solvent: A fundamental approach. *J. Comput. Phys.*, 97(1):144–171, 1991.
[40] B. J. Yoon and A. M. Lenhoff. A boundary element method for molecular electrostatics with electrolyte effects. *J. Comput. Chem.*, 11(9):1080–1086, 1990.
[41] S. S. Kuo, M. D. Altman, J. P. Bardhan, B. Tidor, and J. K. White. Fast methods for simulation of biomolecule electrostatics. In *International Conference on Computer Aided Design (ICCAD)*, 2002.
[42] M. D. Altman, J. P. Bardhan, B. Tidor, and J. K. White. FFTSVD: A fast multiscale boundary-element method solver suitable for BioMEMS and biomolecule simulation. *IEEE T. Comput.-Aid. D.*, 25:274–284, 2006.
[43] G. C. Hsiao and R. E. Kleinman. Error analysis in numerical solution of acoustic integral equations. *International Journal for Numerical Methods in Engineering*, 37:2921–2933, 1994.
[44] J. P. Bardhan, M. G. Knepley, and P. Brune. Public mercurial repository containing all source code in supplementary material. https://bitbucket.org/jbardhan/matlab-analytical-nonlocal-sphere.
[45] L. W. Cai. On the computation of spherical Bessel functions of complex arguments. *Comp. Phys. Comm.*, 182:663–668, 2011.
[46] J. Van Bladel. *Electromagnetic Fields*. John Wiley & Sons, Hoboken, NJ, second edition, 2007.
[47] M. V. Fedorov and A. A. Kornyshev. Unravelling the solvent response to neutral and charged solutes. *Molecular Physics*, 105:1–16, 2007.
[48] A. A. Kornyshev and J. Ulstrup. Polar solvent structural parameters from protonation equilibria of aliphatic and alicyclic diamines and from absorption bands of mixed-valence transition-metal complexes. *Chemical Physics Letters*, 126, 1986.

[49] D. Xie, Y. Jiang, P. Brune, and L. R. Scott. A fast solver for a nonlocal dielectric continuum model. *SIAM Journal of Scientific Computing*, 34:B107–B126, 2012.
[50] M. Nina, W. Im, and B. Roux. Optimized atomic radii for protein continuum electrostatics solvation forces. *Biophys. Chem.*, 78:89–96, 1999.
[51] J. P. Bardhan, P. Jungwirth, and L. Makowski. Affine-response model of molecular solvation of ions: Accurate predictions of asymmetric charging free energies. *J. Chem. Phys.*, 137:124101, 2012.
[52] Henry S. Ashbaugh. Convergence of molecular and macroscopic continuum descriptions of ion hydration. *The Journal of Physical Chemistry B*, 104(31):7235–7238, 2000.
[53] A. A. Rashin and B. Honig. Reevaluation of the Born model of ion hydration. *J. Phys. Chem.*, 89:5588–5593, 1985.
[54] I. S. Joung and T. E. Cheatham III. Determination of alkali and halide monovalent ion parameters for use in explicitly solvated biomolecular simulations. *J. Phys. Chem. B*, 112:9020–9041, 2008.
[55] W. L. Jorgensen, J. Chandrasekhar, J. D. Madura, R. W. Impey, and M. L. Klein. Comparison of simple potential functions for simulating liquid water. *J. Chem. Phys.*, 79:926–935, 1983.
[56] H. J. C. Berendsen, J. R. Grigera, and T. P. Straatsma. The missing term in effective pair potentials. *The Journal of Physical Chemistry*, 91(24):6269–6271, 1987.
[57] H. Gong, G. Hocky, and K. F. Freed. Influence of nonlinear electrostatics on transfer energies between liquid phases: Charge burial is far less expensive than Born model. *Proc. Natl. Acad. Sci. USA*, 105:11146–11151, 2008.
[58] A. Mukhopadhyay, A. T. Fenley, I. S. Tolokh, and A. V. Onufriev. Charge hydration asymmetry: the basic principle and how to use it to test and improve water models. *J. Phys. Chem. B*, 116:9776–9783, 2012.
[59] S. Rajamani, T. Ghosh, and S. Garde. Size dependent ion hydration, its asymmetry, and convergence to macroscopic behavior. *J. Chem. Phys.*, 120:4457, 2004.
[60] D. L. Mobley, K. A. Dill, and J. D. Chodera. Treating entropy and conformational changes in implicit solvent simulations of small molecules. *J. Phys. Chem. B*, 112:938–946, 2008.
[61] Y. Y. Sham, I. Muegge, and A. Warshel. The effect of protein relaxation on charge-charge interactions and dielectric constants of proteins. *Biophys. J.*, 74(4):1744–1753, 1998.
[62] C. N. Schutz and A. Warshel. What are the dielectric constants of proteins and how to validate electrostatic models? *Proteins*, 44:400–417, 2001.
[63] M. Gilson and B. Honig. The dielectric constant of a folded protein. *Biopolymers*, 25:2097–2119, 1986.
[64] E. Demchuk and R. C. Wade. Improving the continuum dielectric approach to calculating pKas of ionizable groups in proteins. *J. Phys. Chem.*, 100:17373–17387, 1996.
[65] J. P. Bardhan. Nonlocal continuum electrostatic theory predicts surprisingly small energetic penalties for charge burial in proteins. *J. Chem. Phys.*, 135:104113, 2011.
[66] J. P. Bardhan and M. G. Knepley. Mathematical analysis of the boundary-integral based electrostatics estimation approximation for molecular solvation: Exact results for spherical inclusions. *J. Chem. Phys.*, 135:124107, 2011.
[67] J. Liang and S. Subramaniam. Computation of molecular electrostatics with boundary element methods. *Biophys. J.*, 73(4):1830–1841, 1997.
[68] G. Sigalov, A. Fenley, and A. Onufriev. Analytical electrostatics for biomolecules: Beyond the generalized Born approximation. *J. Chem. Phys.*, 124(124902), 2006.
[69] J. F. Ahner and R. F. Arenstorf. On the eigenvalues of the electrostatic integral operator. *Journal of Mathematical Analysis and Applications*, 117:187–197, 1986.
[70] J. F. Ahner, V. V. Dyakin, V. Ya. Raevskii, and St. Ritter. Spectral properties of operators of the theory of harmonic potential. *Mathematical Notes*, 59(1):3–11, 1996.
[71] J. P. Bardhan and M. G. Knepley. Computational science and re-discovery: open-source implementation of ellipsoidal harmonics for problems in potential theory. *Computational Science and Discovery*, 5:014006, 2012.